© 2023. Published by The Company of Biologists Ltd | Development (2023) 150, dev201865. doi:10.1242/dev.201865

HUMAN DEVELOPMENT

TECHNIQUES AND RESOURCES ARTICLE

Human pluripotent stem cell-derived inner ear organoids recapitulate otic development *in vitro*

Daniela Doda[1,2,*], Sara Alonso Jimenez[1,2,*], Hubert Rehrauer[2,3], Jose F. Carreño[1,2,3], Victoria Valsamides[1,2], Stefano Di Santo[4], Hans R. Widmer[4], Albert Edge[5,6,7], Heiko Locher[8,9], Wouter H. van der Valk[8], Jingyuan Zhang[10,11], Karl R. Koehler[10,11,12] and Marta Roccio[1,2,‡]

ABSTRACT

Our molecular understanding of the early stages of human inner ear development has been limited by the difficulty in accessing fetal samples at early gestational stages. As an alternative, previous studies have shown that inner ear morphogenesis can be partially recapitulated using induced pluripotent stem cells directed to differentiate into inner ear organoids (IEOs). Once validated and benchmarked, these systems could represent unique tools to complement and refine our understanding of human otic differentiation and model developmental defects. Here, we provide the first direct comparisons of the early human embryonic otocyst and fetal sensory organs with human IEOs. We use multiplexed immunostaining and single-cell RNA-sequencing to characterize IEOs at three key developmental steps, providing a new and unique signature of *in vitro*-derived otic placode, epithelium, neuroblasts and sensory epithelia. In parallel, we evaluate the expression and localization of crucial markers at these equivalent stages in human embryos. Together, our data indicate that the current state-of-the-art protocol enables the specification of bona fide otic tissue, supporting the further application of IEOs to inform inner ear biology and disease.

KEY WORDS: Inner ear development, Human iPSC-derived inner ear organoids, Human otocyst, Sensory epithelia, Hair cells, Otic neuroblasts

[1]Inner Ear Stem Cell Laboratory, Department of Otorhinolaryngology, Head and Neck Surgery, University Hospital Zurich (USZ), 8091 Zurich, Switzerland. [2]Department of Otorhinolaryngology, Head and Neck Surgery, University of Zurich (UZH), 8006 Zurich, Switzerland. [3]Functional Genomics Center Zurich (ETH Zurich and University of Zurich), 8092 Zurich, Switzerland. [4]Program for Regenerative Neuroscience, Department for BioMedical Research, University of Bern, 3008 Bern, Switzerland. [5]Eaton Peabody Laboratory, Massachusetts Eye and Ear, Boston, MA 02114, USA. [6]Department of Otorhinolaryngology - Head and Neck Surgery, Harvard Medical School, Boston, MA 02115, USA. [7]Harvard Stem Cell Institute, Cambridge, MA 02138, USA. [8]OtoBiology Leiden, Department of Otorhinolaryngology and Head & Neck Surgery, Leiden University Medical Center, 2333 ZA Leiden, the Netherlands. [9]The Novo Nordisk Foundation Center for Stem Cell Medicine (reNEW), Leiden University Medical Center, 2333 ZA Leiden, the Netherlands. [10]Department of Otolaryngology, Boston Children's Hospital, Boston, MA 02115, USA. [11]F.M. Kirby Neurobiology Center, Boston Children's Hospital, Boston, MA 02115, USA. [12]Department of Plastic and Oral Surgery, Boston Children's Hospital, Boston, MA 02115, USA.
*These authors contributed equally to this work

‡Author for correspondence (marta.roccio@usz.ch)

D.D., 0009-0005-6237-6331; H.R., 0000-0001-7612-9394; V.V., 0000-0001-5486-7417; S.D.S., 0000-0002-4032-999X; H.R.W., 0000-0003-3378-8765; A.E., 0000-0001-8641-755X; H.L., 0000-0002-4174-0270; W.H.v.d.V., 0000-0001-5661-7796; J.Z., 0000-0002-7968-629X; K.R.K., 0000-0002-0685-538X; M.R., 0000-0001-7568-9429

Handling Editor: James Wells
Received 12 April 2023; Accepted 1 August 2023

INTRODUCTION

The inner ear contains six distinct epithelial sensory patches that detect head movement- and sound-induced fluid vibration and act as peripheral receptors for the senses of balance and hearing. Sensory epithelia (SE) comprise two cell types: supporting cells and hair cells (HC). The latter function as mechanoreceptors. Mechanical deflection of stereocilia bundles in the apical domain of HC results in cellular depolarization and neurotransmitter release on the basal side. This in turn, activates the afferent fibers of the cochlear or vestibular neurons in direct synaptic contact with them, which subsequently relay to the upper auditory centers. Sensory and non-sensory epithelia, as well as the cochleovestibular neurons, have a common developmental origin in the otic vesicle (OV) or otocyst (Alsina and Whitfield, 2017; Groves and Fekete, 2012). The OV is derived from the invagination of the otic placode (OP) into the underlying mesenchyme. The OV forms around the fourth week of human embryo development (O'Rahilly, 1963), and in mice around embryonic day (E) 8.5 to E9 (O'Rahilly, 1963; Wu and Kelley, 2012).

The OP is one of the posterior placodes (Saint-Jeannet and Moody, 2014). Cranial placodes are specified from a transient pre-placodal ectoderm (PPE) region that develops at the neural border, between the neural plate and non-neural ectoderm (NNE) (Litsiou et al., 2005; Martin and Groves, 2006; Saint-Jeannet and Moody, 2014; Steventon et al., 2014). This is further patterned along the anterior-posterior axis of the developing head and subdivides into distinct placodes giving rise to the lens, the nasal/olfactory, the trigeminal, the adenohypophyseal, the otic and the epibranchial placodes. The OP is characterized by the expression of genes such as *PAX8* and *PAX2*, which are also required for inner ear morphogenesis (Bouchard et al., 2010). Upon invagination and detachment from the surface ectoderm, complex morphogenetic events lead to the generation of the inner ear membranous labyrinth and its specialized sensory organs (Groves and Fekete, 2012; Wu and Kelley, 2012). Morphogens secreted by the hindbrain, the mesenchyme and the floor plate generate the coordinates for the anterior-posterior, the lateral-medial and the dorsal-ventral axis in the OV and result in the specification of sensory and non-sensory regions, as well as cochlear or vestibular fate (Bok et al., 2007; Durruthy-Durruthy et al., 2014; Riccomagno et al., 2005; Wu and Kelley, 2012).

The ventral portion of the OV contains SOX2-expressing progenitors that form the so-called pro-neurosensory domain (Kiernan et al., 2005; Puligilla et al., 2010; Steevens et al., 2017). This area gives rise to both the SE and the neural components of the inner ear. Neuroblasts delaminate from the pro-neurosensory region (Evsen et al., 2013; Puligilla et al., 2010; Radde-Gallwitz et al., 2004; Steevens et al., 2017) and coalesce to form the cochleovestibular ganglion (CVG), which will further innervate

Development (2023) 150, dev201865. doi:10.1242/dev.201865

the sensory patches. In mouse development this occurs at ∼E9.5-E10 (Appler and Goodrich, 2011). The prosensory region within the otocyst further segregates into distinct prosensory domains which give rise to the SE in the ampullae of the semicircular canals, to the maculae of the utricle and saccule and to the sensory epithelium in the cochlear duct (Gu et al., 2016). Migrating cranial neural crest (CNC) infiltrates the OV and surrounding otic mesenchyme and contributes to the population of glial/Schwann cells in the cochlear and vestibular ganglia (Mendez-Maldonado et al., 2020; Renauld et al., 2022) and to the intermediate cell layer in the stria vascularis (Adameyko et al., 2012; Cable et al., 1992; Locher et al., 2015; Renauld et al., 2022; Steel and Barkway, 1989). CNC-derived mesenchyme instead gives rise to the ossicles of the middle ear (Martik and Bronner, 2021).

Our knowledge of these early developmental events is almost exclusively based on studies performed in model organisms such as the mouse and the chick; it is unclear how similarly these processes play out in humans. We and others have shown that the appearance of the first HC in the vestibular organs occurs around weeks 8-10 of human development. However, in the cochlea, these develop a few days later, starting at week 11 with a basal to apical gradient (Lavigne-Rebillard and Pujol, 1986; Locher et al., 2014, 2013; Pechriggl et al., 2015; Pujol and Lavigne-Rebillard, 1985; Roccio et al., 2018; Sans and Dechesne, 1985). By week 20, hair bundles can be observed (Lavigne-Rebillard and Pujol, 1987, 1988) and *in utero* hearing starts during the third trimester.

Using multiplexed qPCR we previously provided the first molecular characterization of the developing cochlear duct, utricular macula and spiral ganglion at weeks 8-12 of fetal development (Roccio et al., 2018). More recent studies exploiting single-cell RNA-sequencing (scRNA-seq) have provided additional insights into the transcriptional profile of the human inner ear components (Shengyang Yu et al., 2019 preprint; van der Valk et al., 2023). Earlier stages of human inner ear development are instead scarcely characterized. Although anatomical studies based on CT scans/MRI (Yasuda et al., 2007) or tissue sectioning followed by 3D reconstruction (de Bakker et al., 2016) and embryology atlases (https://www.3dembryoatlas.com; https://www.ehd.org/virtual-human-embryo/) give us a picture of morphological events during early otocyst/inner ear development, the molecular characterization of this process is limited. Major experimental, logistic and ethical limitations remain, which hamper the availability and accessibility to human fetal/embryonic inner ear tissue.

State-of-the-art inner ear organoid (IEO) protocols based on stem cell differentiation in 3D culture recapitulate many features of inner ear morphogenesis *in vitro* (Koehler et al., 2017; Munnamalai and Fekete, 2017; van der Valk et al., 2021). Pluripotent stem cells are guided in a stepwise fashion towards the otic lineage, eventually leading to multicellular aggregates bearing sensory and non-sensory inner ear epithelia and otic-like neurons (Koehler et al., 2017; Nie and Hashino, 2020). IEOs are a powerful tool to refine our understanding of the molecular signals leading to inner ear cell type specification. Benchmarking these models to the primary human tissue would provide a robust base for their future use to study organ development and model diseases. In addition, reliable models of the human inner ear could allow for testing novel therapeutic strategies for sensorineural hearing loss and vestibular disorders (Nist-Lund et al., 2022; Roccio and Edge, 2019).

Here, we have compared for the first time a set of human embryos from Carnegie stage (CS) 11 to 13 (week 4-5 of embryonic development) with *in vitro* stages of IEO differentiation. We observed the expression of shared genes and protein markers between CS11 human embryos and early-stage IEOs (day 8-12 *in vitro*). OV-like structures and neuroblasts derived *in vitro* at days 20-40 showed remarkable similarity to CS13 embryos. Finally, sensory vesicles matured to days 50-60 were comparable with weeks 10-12 inner ear fetal specimens. Our findings indicate that IEOs faithfully recapitulate otic developmental steps by generating the progenitors of the inner ear sensory and non-sensory lineages, and they provide a solid foundation for future studies of human inner ear biology.

RESULTS

Characterization of the developing human otocyst

The invagination of the OP into the head mesenchyme is a crucial event leading to the formation of the OV. This occurs around day 20 of human development (CS10-11) (de Bakker et al., 2016). Remarkably, two of the earliest fetal samples we collected (staged CS11, ∼24-25 days) provided a snapshot of OV formation and displayed otic pits in the process of pinching off from the surface ectoderm. We immunostained the CS11 specimens and later samples at CS12 (26-30 days) and CS13 (28-32 days) with markers of OV development (SOX2, PAX2, PAX8, SOX10), neural epithelium and new-born neurons (PAX6, TUBB3, NEUROD1) and neural crest (SOX10) to provide an initial molecular characterization of these samples (Figs 1 and 2; Fig. S1).

During this early developmental window, SOX2 expression is detectable in the developing CNS, as well as in the otocyst. In the latter, SOX2 staining appears to be predominantly localized in the anteroventral portion (Figs 1A-C, 2A-C; Fig. S1B). This is particularly obvious in sections at CS13, where the dorsal region of the otocyst/developing inner ear becomes visible (Fig. 1C, panel 4), and it is in agreement with the pattern of expression in the murine otocyst (Gu et al., 2016; Steevens et al., 2017). βIII Tubulin (TUBB3) is undetectable in CS11 samples and starts to appear at CS12 (Fig. 1; Fig. S1E). Here, TUBB3^{+} cells appear in the region of the developing CVG. TUBB3 becomes clearly expressed in the CVG, other cranial ganglia, dorsal root ganglia (DRG), as well as in the developing brain by CS13 (Fig. S1E). At this stage, CVG neurons project to the brainstem (Fig. 1C, panel 4).

PAX2 expression is visible in the OV at CS11 (Fig. 2A). However, the staining becomes more selective in the otocyst by CS13 (Fig. 2C). PAX2 can also be detected in different areas of the developing brain at all stages (Fig. 2A-C). PAX8, instead, is expressed in the otocyst from CS11 to CS13 and it is also present in the mid-hindbrain boundary region, as previously reported in mice (Bouchard et al., 2010) (Fig. 2D-F), and in other cranial ganglia and in the optic vesicle (Fig. S1H). Immunolabeling for SOX10 shows that, at early stages (CS11), this labels almost exclusively neural crest cells in the developing CVG area, while its expression in the OV starts to be detectable at CS12-13 (Fig. 2D-F).

Induction of placode tissue from human iPSC

We then turned to a previously reported protocol to guide the differentiation of human induced pluripotent stem cells (iPSCs) towards otic fate (Koehler et al., 2017; Nie and Hashino, 2020) with the goal of comparing otic tissue derived from iPSCs with the human samples. As in previous studies, different requirements for exogenous BMP4 have been reported in human embryonic stem cells (hESCs) and human iPSCs. We tested varying concentrations of BMP4 (from 0 ng/ml to 10 ng/ml) (Fig. 3; Fig. S2) to optimize placode induction. Substantial morphological differences are already observed at day 4 *in vitro* (Fig. S2A). In the absence of

Development (2023) 150, dev201865. doi:10.1242/dev.201865

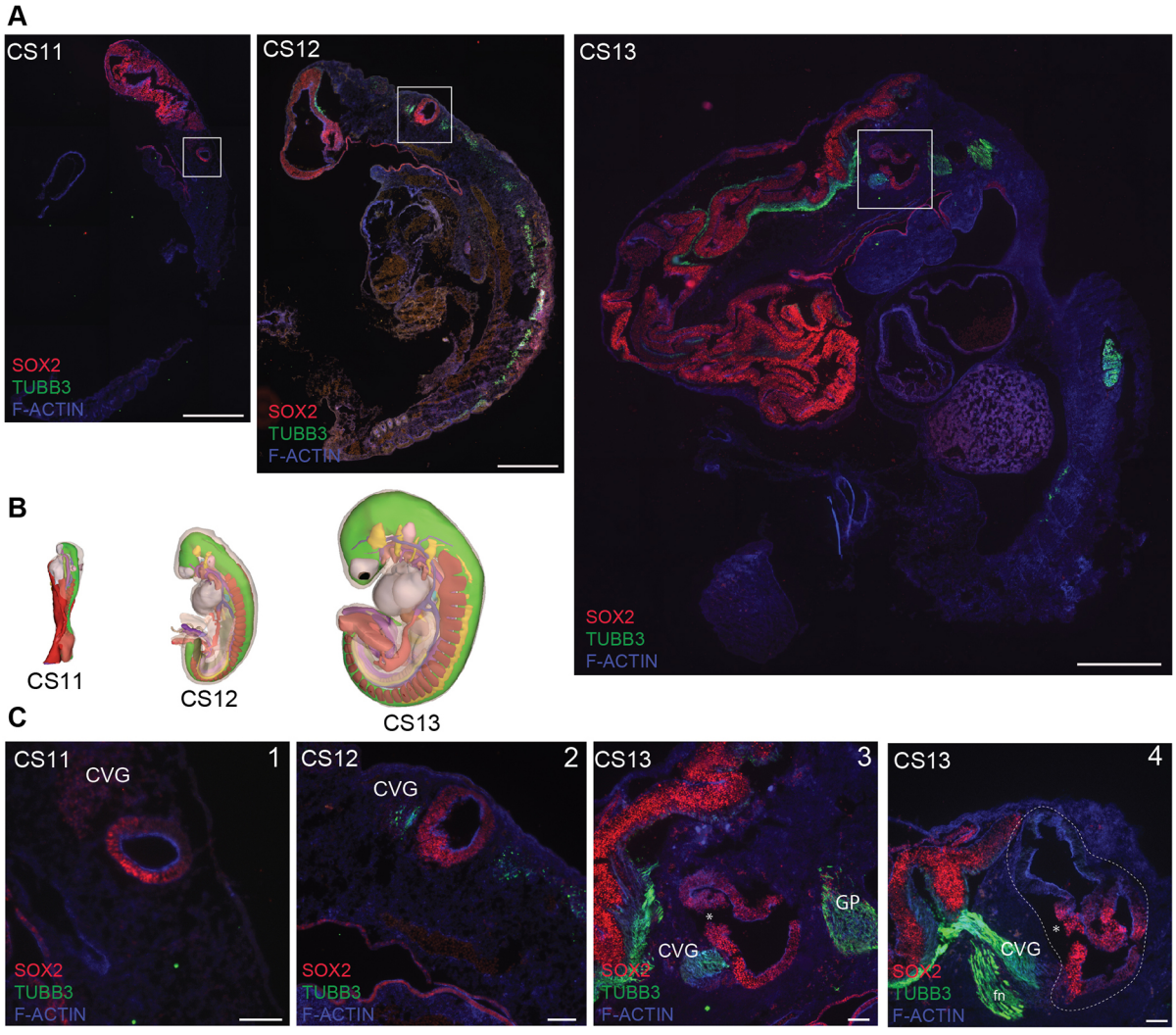


Fig. 1. Otic vesicle development in human embryos. (A) Human fetal samples at CS11 (E1026), CS12 (E1027) and CS13 (E1037) immunolabelled to detect the developing otocysts (white box) with SOX2, TUBB3 and F-Actin (Phalloidin). (B) 3D reconstructions of embryos at CS11 (day 23-26), CS12 (day 26-30) and CS13 (day 28-32) adapted from the 3D Embryo Atlas (https://www.3dembryoatlas.com). (C) Higher magnification of the otocyst and the developing cochleo-vestibular ganglion (CVG) stained with SOX2 and TUBB3 antibodies and F-Actin (Phalloidin). Panels 3 and 4 show sections at different lateral-medial levels of the same sample (E1037). Asterisk indicates potential cutting artifact or tissue damage. fn, putative branch of the facial nerve; GP, glossopharyngeal ganglion. Scale bars: 1 mm (A); 100 µm (C).

BMP4, the formation of a thick ectoderm layer can be observed, compatible with neural ectoderm induction (Lancaster et al., 2013). Concentrations between 1 and 2.5 ng/ml induce a thinner and ruffling outer ectoderm layer, as previously reported (Koehler et al., 2017; Nie and Hashino, 2020). For BMP4 levels of 5 ng/ml or more, organoids have a round morphology, a very thin cellular layer at the periphery of the organoid and most cells concentrated in the core. To correlate these features with molecular markers, we assessed the expression of the pan-placodal marker SIX1 and cadherin 1 (CDH1). Co-expression was used to evaluate placode induction. Although optimal concentrations were cell-line specific (Fig. 3A PAX2-GFP line and Fig. 3B SOX2-GFP line), BMP4 levels ranging between 1 ng/ml and 2.5 ng/ml generate, in all three lines, placodal ectoderm (PE) at the surface of the aggregate (Fig. 3; Fig. S2B). To confirm proper exposure to BMP4, samples were stained with an antibody recognizing the downstream target phospho-SMAD, showing a dose-dependent increase in phosphorylation of SMAD1-5-9 proteins (p-SMAD) (Fig. 3; Fig. S2C). To better characterize this system, we further analyzed the fate of the organoids cultured in the absence of exogenous BMP: BMP4 (0 ng/ml). Neither of the cell lines tested upregulates NNE/PE markers (TFAP2A, CDH1, SIX1). Instead, we observed neuronal progenitors (SOX2, NEUROD1, Ki67), neurons (CDH2, TUBB3) and neural crest-derived glia (CDH2, SOX10) (Fig. S2E; see also data in Fig. S7A,B discussed later). In response to high levels of BMP (5-10 ng/ml), the expression of GATA3, p63 and CDH1, is observed, suggesting that the NNE has committed to surface ectoderm/epidermal fate (Fig. S2D).

Transcriptional characterization of the placodal tissue in IEOs

In order to characterize in depth the placodal tissue, as well as the cellular composition of the organoids at this stage, we employed scRNA-seq. First, we assessed the percentage of epithelial cells differentiated at day 8 by flow cytometry analysis. As 40.57%±9.4 (mean±s.d.; n=4 independent experiments) of cells expressed the epithelial marker EPCAM, we decided to analyze whole organoids, expecting we would get enough coverage of the placode tissue of

Development (2023) 150, dev201865. doi:10.1242/dev.201865

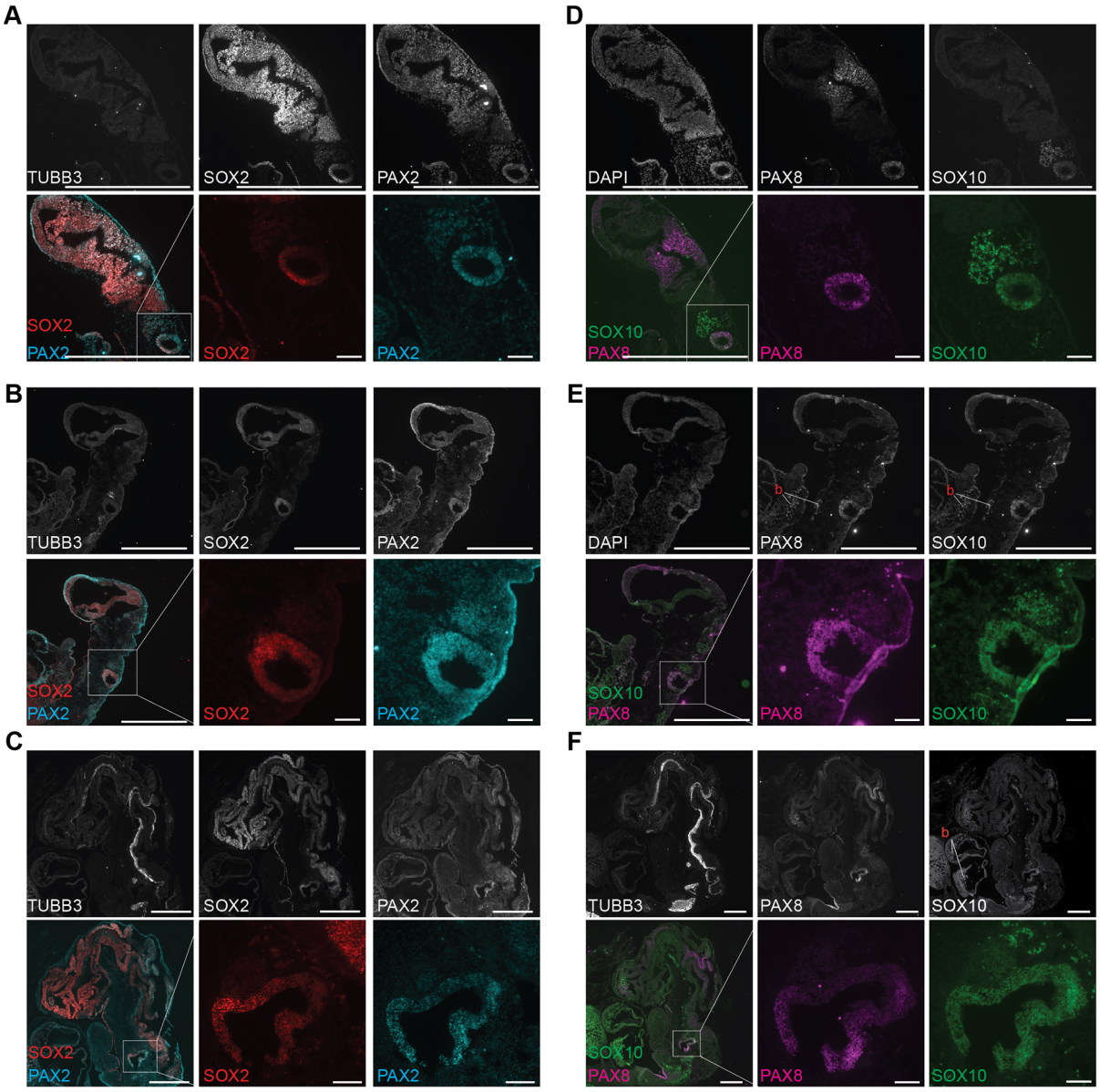


Fig. 2. Characterization of otic vesicle development in human embryos. (A-F) Human fetal samples at CS11 (E1026; A,D), CS12 (E1027; B,E) and CS13 (E1037; C,F) immunolabelled to detect the developing otocysts with SOX2, PAX2 and TUBB3 staining (left) or SOX10, PAX8 and TUBB3 staining (right). A tile scan of the head region (top; scale bars: 1 mm) and a detail of the otocyst (bottom; scale bars: 100 µm) are shown for each panel; all images are consecutive sections to those shown in Fig. 1. b in E and F indicates autofluorescence blood cells.

interest as well as of the co-developed cell types. After data filtering (see Materials and Methods), 15,002 cells were analyzed from 200 pooled day 8 organoids derived from the SOX2-GFP iPSC line.

The two major cell populations that were identified consisted of an epithelial component (*EPCAM*$^{+}$ and *CDH1*$^{+}$), representing ∼70% of all cells, and a remaining mesenchymal/neuronal component (*EPCAM*$^{-}$and *CDH1*$^{-}$) (Fig. 4A-E; Fig. S3). The two major groups of epithelial cell clusters included PE-like cells and surface ectoderm-like cells (Fig. 4A,B). The PE cluster expresses the epithelial markers *EPCAM* and *CDH1*, in addition to *CDH2* and *SIX1* (Fig. 4D,E; Fig. S3A). Overall, this 'pan-placodal' population represents 47% of all cells. Among the markers distinctive for PE cells identified in the scRNA-seq experiment, we found *SPARCL1* and *BMP4* (Fig. 4F).

Six PE subclusters can be distinguished by unsupervised clustering. Cells expressing posterior/otic epibranchial placode (OEPD) markers (subclusters PE5, PE7, PE9) represent 21% of total cells (and 43% of the PE population) and express *PAX8*. In addition, these cells express *FGF3* and *FGF8*. Both genes were previously reported as important for otic development in different vertebrates (Hidalgo-Sanchez et al., 2000; Leger and Brand, 2002; Maroon et al., 2002; Zelarayan et al., 2007). We did not detect *PAX2* nor *SOX10* expression at day 8 in this cell population (Fig. 4D,E). Both genes become upregulated at later stages in the otic epithelium (OE; see Fig. 5). The clusters PE0 and PE1 include cells expressing OTX1 (12% of PE), OTX2 (16% of PE) and PAX3 (5% of PE), potentially representing anterior placode (AP) cells at this stage (Baker et al., 1999; Steventon et al., 2012) (Fig. 4F).

Development (2023) 150, dev201865. doi:10.1242/dev.201865

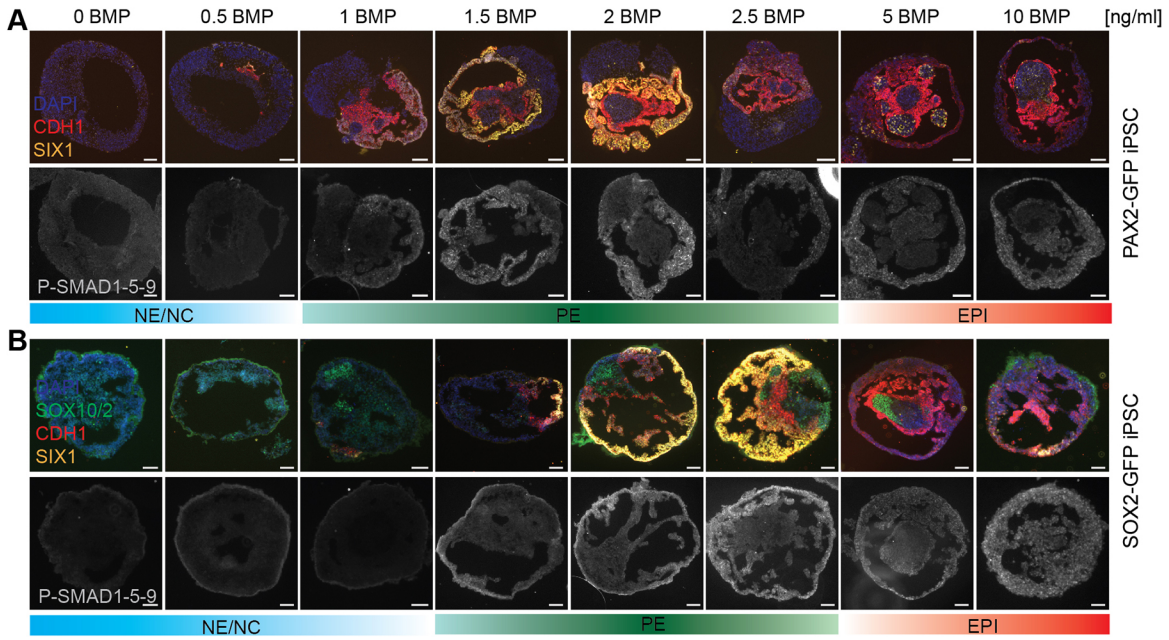


Fig. 3. Placode induction in IEOs is dependent on BMP concentration. (A) iPSC aggregates derived from the PAX2-GFP iPSC line exposed to discrete BMP concentrations (0-10 ng/ml) from day 0 to day 3.5 of culture. Organoids fixed at day 8 and immunostained for the placodal marker SIX1 and co-stained with CDH1 (top panels) or phosphorylated SMAD1-5-9 (bottom panels). (B) iPSC aggregates derived from the SOX2-GFP iPSC line exposed to discrete BMP concentration (0-10 ng/ml) from day 0 to day 3.5 of culture. Organoids fixed at day 8 and immunostained for the placodal marker SIX1 and co-stained with CDH1 and SOX10 (top panels) or phosphorylated SMAD1-5-9 (bottom panels). Placodal ectoderm (PE) forms for concentrations of 1-2.5 ng/ml, with cell line-specific optimal levels. EPI, epidermis; NE/NC, neural epithelium/neural crest. Scale bars: 100 µm.

The other cellular components detected in the dataset include surface ectoderm-like cells, 22% of the total cell number (Fig. 4A,B), expressing several NNE/epidermal markers: *CDH1*, *EPCAM*, *GATA3*, *TFAP2A*, *ISL1*, *HAND1*, *KRT18* and *KRT8* (Fig. S3C). Among the non-epithelial clusters, the following populations were found (Fig. S3C): (1) a neural crest (NC) population (1%), which we classified based on the expression of genes such as *SOX10*, *PAX3*, *PLP1* and *FOXD3*; (2) NC-derived mesenchyme (Soldatov et al., 2019) (24%), which, in addition to NC markers, shows upregulation of epithelial-to-mesenchymal transition (EMT) markers (*PRRX1*, *SNAI1*, *TWIST1/2* and *VIM*) (clusters MES4-MES6-MES8); (3) a small population of neurons (1%) positive for *NEUROD1*, *NEUROD4*, *NEUROG1*, *ISL1* and *TUBB3*, also expressing a number of placodal genes, suggesting they may be placode-derived newborn neurons (Durruthy-Durruthy et al., 2014); (4) a cluster of *CDH2*$^{+}$ and *SOX2*$^{+}$ neural-epithelial cells (5% of total), with two distinct gene expression subclusters, one with high expression of *PAX6* and *OTX1/2* and the other expressing *PAX2* and *PAX8* (Fig. S3C).

Overall, the protocol yields a distinct cell population of placodal ectoderm which includes cells with a posterior/OEPD signature. The other populations derived in our cultures agree with the expected 'off-target' tissue generated by the protocol (Koehler et al., 2017), possibly receiving insufficient or excessive BMP signal activation, as reported in Fig. S2.

Placode characterization and comparison with human samples

To confirm the transcriptional data, we implemented immunostaining of consecutive sections and exploited tile-scanning to evaluate marker expression across conditions and time points (Fig. S4A). By day 4 or differentiation, the outer epithelial layer expressed CDH1, CDH2, TFAP2A and SIX1 and lacked PAX2, PAX6 and SOX10 expression. Sparse SOX10^{+} NC cells were detected in the core of the organoid (Fig. S4B). Using the SOX2-GFP reporter line, we observed that the core also expressed GFP. This could represent remaining SOX2^{+} pluripotent cells or neuronal progenitors. SIX1 expression was further maintained at days 8 and 12 on the surface of the aggregate (Fig. S4C). Starting at day 8, the otic marker PAX8 was upregulated in the outer layer of the organoids in cells that still co-expressed CDH1, CDH2, EPCAM, TFAP2A and SIX1 (Fig. 4G). We could not convincingly detect PAX2 expression in the PE layer at this time point. PAX2 expression in the OP is also slightly delayed compared with PAX8 expression in mouse otocyst development (Bouchard et al., 2010). Some PAX6^{+} neural epithelial cells were identified in the core of the organoids together with SOX10^{+} NC cells and SOX2^{+} neuronal progenitor cells (Fig. 4G). This pattern of marker expression was maintained up to day 12 (Fig. S4C). We also evaluated the expression of SPARCL1, which indeed was observed in the outer epithelial layer in day 8-12 organoids (Fig. S4D). Overall, the cellular composition identified by immunostaining matches the scRNA-seq characterization, with the identified placodal layer positioned at the organoid surface.

We then stained CS11 embryos (days 24-25) for the same marker panel (Fig. 4H). The *in vivo* time point represents a slightly later developmental stage, nevertheless, many of the placodal markers were similarly expressed, including CDH1, CDH2, SIX1, PAX8 and TFAP2A. PAX6 was only detected in the developing brain and not in the otocyst (Fig. 4H; Fig. S1B). As shown in Fig. 2, SOX10 staining at this stage mostly labelled NC cells in the region of the developing CVG, but not the epithelial components of the otocyst, as found in the organoids.

Otic vesicle characterization

As a next step, we characterized by transcriptional profiling otic tissue differentiated within the organoid after 20-30 days of culture.

Development (2023) 150, dev201865. doi:10.1242/dev.201865

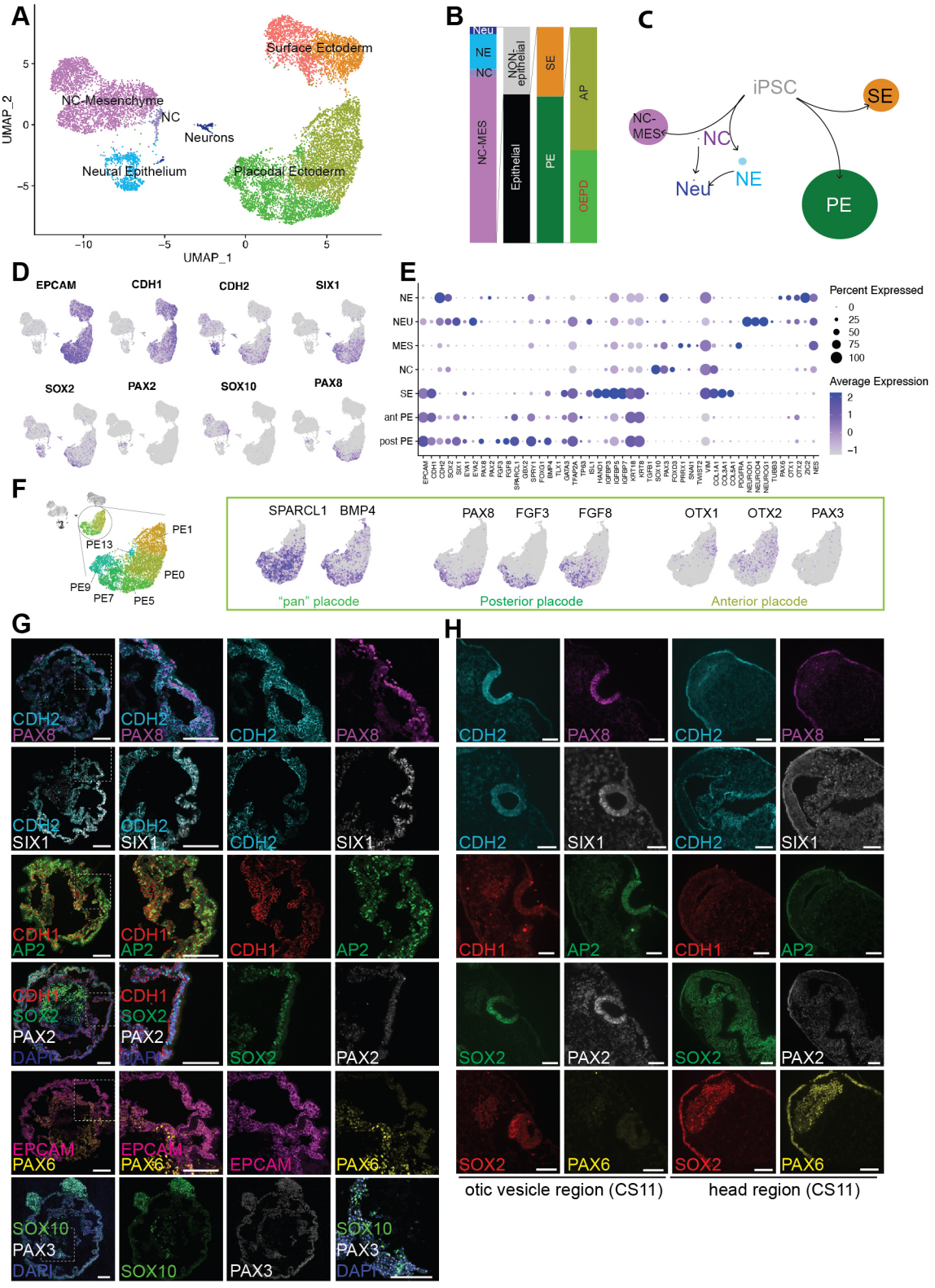


Fig. 4. See next page for legend.

Again, we first estimated the percentage of epithelial cells by staining IEO sections or dissociated cultures with an antibody recognizing EPCAM. Epithelial cells represented 8.6%±0.7 (s.d.) (n=2 experiments; day 27 and day 30) of total cells, when assessed by flow cytometry, and 5.7±2.5 (n=2 experiments; day 30) by image analysis. To increase the yield of otic progenitors for single-cell analysis, we therefore decided to sort EPCAM$^+$ cells. We pooled together 140 organoids at day 26 of differentiation for dissociation to single cells. EPCAM$^+$ cells were sorted (Fig. 5A,B) and loaded on the 10x Chromium. Eventually 11,793 cells were analyzed

Development (2023) 150, dev201865. doi:10.1242/dev.201865

Fig. 4. Comparison placodal tissue differentiated in IEO and CS11 samples. (A) UMAP plot of day 8 scRNA-seq data showing the identified cell clusters: placodal ectoderm (PE; green), surface ectoderm (SE; orange), neural crest (NC; violet), NC-mesenchyme (NC-MES; magenta), neural epithelium (NE; turquoise), neurons (Neu; blue). (B) Histogram plot showing the relative abundance of the different populations at day 8. AP, anterior placode; OEPD, otic-epibranchial placode. (C) Schematic of the potential differentiation dynamics. Size of the circles is proportional to the percentage of cells in the cluster, relative to total number of cells. (D) UMAP plots with selected marker genes defining the PE cluster. (E) Dot plot for selected markers for the main clusters. ant PE, anterior placode (PE0, PE1; PE13); post PE, posterior placode (PE5, PE7, PE9). (F) UMAP plots for the PE population only (manual selection). Six subclusters are identified by unsupervised clustering: PE0, PE1, PE9, PE7, PE5, PE13. 'Pan' placodal, anterior or posterior placode markers are shown. (G) Organoid characterization at day 8. Immunofluorescent staining characterization on consecutive sections was used to verify the expression/absence of the following markers: CDH1, CDH2, SIX1, TFAP2A (AP2), PAX8, PAX2, SOX2, PAX6, SOX10, PAX3. Boxed areas are imaged at higher magnification and shown as merged and single channels. (H) Images of the OV (left) and head/developing brain (right) in CS11 embryos (E1026) immunostained for PAX8, SIX1, CDH1, TFAP2A, SOX2 and PAX6. Different lateral to medial sections are shown from the same embryo. OV and head regions are from the same section and imaged with the same parameters to compare signal intensity. Scale bars: 100 µm.

(Fig. 5C-H; Fig. S5). The great majority of cells expressed EPCAM (Fig. 5C). Two major epithelial clusters were identified in the dataset: (1) OE, which represented 43.12% of all cells, and (2) epithelial cells with an epidermal-like signature (EP), representing 43.7% of the total (Fig. 5D,E). The OE derived *in vitro* co-expressed *CDH1* and *CDH2*, whereas the latter was absent in the EP clusters (Fig. 5F; Fig. S5A). OE further expressed high levels of *OC90*, *FBXO2*, *LMX1A* and *TBX2*, as previously identified in mouse studies (Durruthy-Durruthy et al., 2014; Hartman et al., 2015; Kaiser et al., 2021; Sun et al., 2022) (Fig. 5F,G; Fig. S5A,D). The placodal genes *SIX1*, *DLX5* and *PAX8* were still expressed; *PAX2* and *SOX10* became clearly upregulated (Fig. 5F; Fig. S5D). Interestingly, the expression of *SOX2* was limited to a subset of OE cells (59%), potentially indicating that both sensory and non-sensory domains are derived *in vitro*. The population of cells expressing high levels of *SOX2* also expressed *JAG1*. In addition, inner ear genes, such as *OTOL1*, *OTOA* and *USH1C* were identified in this cell population (Fig. 5G). Unsupervised clustering identified five distinct OE subclusters (Fig. S5B), we could however not differentiate them based on the expression of the above-mentioned marker genes.

Interestingly, we were able to distinguish a population of putative otic neuroblasts (ONB) (7.6% of total cells sequenced), expressing low levels of EPCAM, which could be co-isolated with this sorting approach (Fig. 5F,H; Fig. S5). These cells expressed markers such as *ISL1*, *SOX2*, *EYA2*, *FGF8*, *GATA3*, *NEUROG1*, *NEUROD1* and *NEUROD4* (Durruthy-Durruthy et al., 2014; Kaiser et al., 2021; Sun et al., 2022). In addition, ONBs started to express neuronal filaments like *TUBB3* and peripherin (*PRPH*), and the neurotrophin receptors *NTRK3* and *NGFR* (also known as *CD271*). *GADD45G*, *HES6* and *INSM1*, recently identified by scRNA-seq in the developing CVG in mice (Sun et al., 2022), were also expressed in the ONB population. Interestingly, markers identified in this latter study to distinguish spiral ganglion neurons (SGNs) from vestibular ganglion neurons were also expressed (*EPHA5*, *SHOX2*, *MYT1*, *CASZ1*), suggesting that the ONB population may resemble developing SGNs.

Finally, a small fraction of EPCAM$^-$ cells was also detected, including neural epithelial cells (1.5% of total) and mesenchyme (4% of total) (Fig. S5A-C). As sorted cells processed for scRNA-seq in this experiment constituted 9.2% of the total cell pool (Fig. 5B), we estimate that OE cells represent on average 4% of the IEO composition at day 26.

To confirm these data, protein expression for OE markers was assessed by immunostaining and quantified across the three cell lines. We immunostained consecutive sections of organoids at day 30 for FBXO2, SOX10, SOX9, PAX2, PAX8, DLX5 and the epithelial markers EPCAM and CDH1 (Fig. 5I; Fig. S6). Image-based quantification at day 30 of differentiation showed that the otic tissue represented on average 2.4±2% of the whole organoid volume. Similar differentiation efficiency and marker expression were observed in the three different cell lines used in this study and different experiments (Fig. 5J).

Finally, we compared a subset of these markers between day 20-40 IEO and CS13 (day 28-32) samples (Fig. 5K; Fig. 2). PAX2 and SOX2 became distinct in the IEO vesicle, matching the *in vivo* expression. SIX1 and CDH2 were expressed both in CS13 samples as well as in day 30 vesicles, confirming also the scRNA-seq data. SOX10 at this time point was expressed in the OVs, as well as in the surrounding glia, whereas ISL1 was absent in the IEO as well as in CS13 samples at the level of the OE. *In vivo* ISL1 was expressed in neuroblasts in the CVG and other cranial ganglia (glosso-pharyngeal ganglion and vagus nerve are shown in Fig. S7D). The population of ISL1$^+$ cells at CS13 expressed the highest level of TUBB3, indicating that ISL1$^+$ cells are newborn neurons. This matched our transcriptional analysis, as well as the histology of IEO (Fig. 5K). At this time point, *in vitro* otic vesicles were surrounded by neurons co-developed in culture. At earlier time points (day 18), these were found organized in ganglia-like structures expressing ISL1 and being intermingled with SOX10$^+$ and NGFR$^+$ cells (Fig. S7A-C).

Sensory vesicle maturation and comparison with the human inner ear

Starting from day 50-60 of IEO culture, HC develop within the organoids. These are organized in SE intercalated to SOX2$^+$ supporting cells and receive innervation by co-developed neurons (Koehler et al., 2017; Nie and Hashino, 2020; Nie et al., 2022). Similar epithelial sensory patches have been obtained with the three cell lines tested in this study (Figs 6A-C and 7A). We collected organoids at day 60 from two independent experiments for scRNA-seq (see Materials and Methods). In both experiments EPCAM$^+$ cells were sorted (Fig. S8A). The two datasets were then integrated for further analysis (Stuart et al., 2019). Despite sorting epithelial cells, some EPCAM$^-$ cells, including mesenchyme, neural epithelium and neurons, were also identified, likely due to a non-stringent gating strategy in experiment 1 (Fig. S8D). These populations were not further analyzed.

Among the epithelial components (EPCAM$^+$), EP formed the most abundant population. A distinct cluster of OE cells (OEP, 498 cells) was identified, expressing very specifically *OC90*, *FBXO2*, *SOX10*, *OTOL1* and *USH1C* (Fig. S8E). As putative HC did not form a separate cluster, we selected cells using the module score feature of Seurat (see Materials and Methods), using gene sets expressed by HC and OEP (Table S3) and selected these two populations for further analysis (Fig. 6D-H). The identified HC not only expressed newborn-HC markers (Burns et al., 2015; Kolla et al., 2020), including *ATOH1*, *POU4F3*, *GFI1*, *CCER2* and *GNG8*, but also genes associated with HC maturation such as *STRC*, *CDH23*, *PCDH15*, *ESPN*, *TMPRSS3* and *OTOF* (Fig. 6F-H; Fig. S8G,I). Among the top differentially expressed genes in HC versus the OEP, we identified *MYO15A*, *USH2A*, *CIB2*, *GRXCR1*

Development (2023) 150, dev201865. doi:10.1242/dev.201865

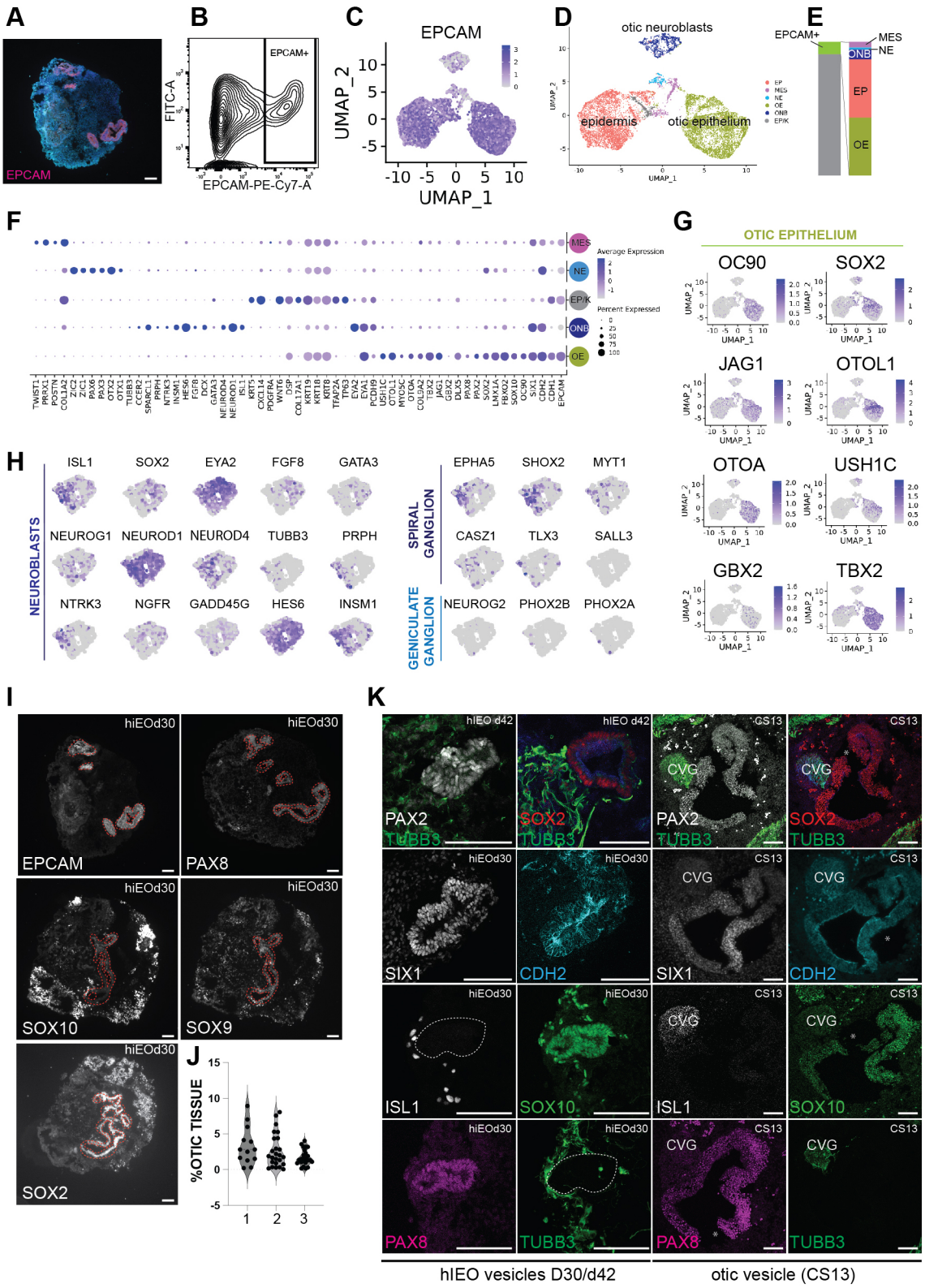


Fig. 5. See next page for legend.

and *PTPRQ*. Many of these genes have been associated with hearing loss before (www.hereditaryhearingloss.org) (Fig. S8I).

We then compared the *in vitro*-generated SE by transcriptional profiling (Fig. 6H) and histological assessment (Fig. 7A; Fig. S9) with human specimens collected at week 12 of development (cochlear samples; Fig. 7B; Fig. S9) or at week 10 (vestibular samples: utricle Fig. 7C; Fig. S9; and saccule Fig. 7D). Comparable expression and localization of MYO7A, SOX2, ESPIN and POU4F3 were observed in HC in the three primary tissues and IEOs (Fig. 7A-D; Fig. S9A,B). In all SE, HC expressed POU4F3,

Development (2023) 150, dev201865. doi:10.1242/dev.201865

Fig. 5. Comparison of otic tissue differentiated in IEO and CS13 samples. (A) EPCAM (magenta) and F-Actin (cyan) staining on an organoid section at day 30 of *in vitro* differentiation. (B) Flow cytometry analysis of cells dissociated at day 26 of differentiation and stained for EPCAM-PeCy7. $EPCAM^+$ cells (9.2% of the total) were sorted and processed for scRNA-seq. (C) UMAP plot of day 26 IEO scRNA-seq showing expression of *EPCAM* in all cells analyzed. (D) UMAP plot of day 26 IEO scRNA-seq with cluster labeling. (E) Percentage of the different cell populations identified by scRNA-seq. (F) Dot plot of the selected populations: mesenchyme (MES; magenta), neural epithelium (NE; turquoise), epidermis/keratinocytes (EP/K; gray), otic neuroblasts (ONB; blue) and otic epithelium (OE; green). (G) UMAP plots of selected genes expressed in the OE cluster. (H) UMAP plots of selected genes labeling the otic neuroblasts cluster (manual selection). (I) Characterization of otic vesicles in SOX2-GFP iPSC line at day 32 of differentiation. The otic markers EPCAM, PAX8, SOX10, SOX9 and SOX2 are shown. Vesicle areas are highlighted with a red contour. (J) Quantification of the organoid area positive for each marker (n=3-4 sections of three organoids per experiment; three independent experiments). No significant differences between the group means (one way ANOVA with multiple comparison). (K) Otic vesicles at day 30-42 of differentiation *in vitro* (hIEOd30, hIEOd42) in comparison with CS13 embryo. CVG, cochleo-vestibular ganglion. Asterisks indicate potential cutting artifact or tissue damage. Scale bars: 100 µm.

a transcription factor of newborn HC, and still expressed SOX2 at this developmental stage (Fig. 7B-D; Fig. S9A) as previously reported (Locher et al., 2013; Roccio et al., 2018). ESPIN labels hair bundles, which both for IEOs and cochlear HC were just starting to appear and had an immature morphology. We did not observe expression of prestin in outer hair cells (OHC) in the cochlear tissue at week 12. A similar faint immunoreactivity was detected in the IEO vesicles (Fig. S9B). In line with this, *SLC26A5*, encoding prestin, was expressed only by a few cells (Fig. 6H). Prestin expression has been reported in later developmental stages than those analyzed here, starting only at postnatal day (P) 9-10 in mice (Hang et al., 2016).

Supporting cells expressed SOX9 and SOX10, in addition to SOX2, in IEOs and in primary tissues. SOX9 expression was higher in the cochlear SE compared with adjacent lateral and medial domains, whereas SOX10 displayed an opposite pattern (Fig. 7B; Fig. S9C). SOX9 was also highly expressed in vestibular SE (Fig. 7C,D; Fig. S9C). A similar pattern was observed in IEOs (Fig. 7A; Fig. S9C). Some non-epithelial $SOX10^+$ cells were detected in the mesenchyme below the SE and in IEOs (Fig. 7C,D, white asterisks), likely labeling glial cells. FBXO2 staining could be observed in the cochlear duct, in the vestibular epithelia and IEOs. Its expression was not restricted to sensory areas, as shown in the murine inner ear (Hartman et al., 2018). We have previously reported the expression of NGFR in the developing human cochlear prosensory domain (Roccio et al., 2018). Interestingly a similar pattern of NGFR expression could be observed in some of the vesicles in the IEOs (Fig. 7A; Fig. S9D, blue arrows).

Finally, *ISL1* transcripts were identified both in HC and in supporting cells (Fig. 7E). Histological analysis of day 60 vesicles showed SE containing $POU4F3^+$ HC co-expressing ISL1, intercalated by $ISL1^+$ supporting cells. A similar expression pattern was observed in the SE of utricle, saccule and cochlea (Fig. S10A).

To assess whether we could further distinguish different HC identities, we analyzed the expression of genes reported in studies comparing cochlear and vestibular SE (Burns et al., 2015; Elkon et al., 2015; Scheffer et al., 2015; Wilkerson et al., 2021) (Fig. 7E). We identified *INSM1*, previously described in cochlear OHC (Elkon et al., 2015; Wiwatpanit et al., 2018) as well *CD164L2*, *SYT14* and *ABCA5*, recently described in adult human vestibular HC (Wang et al., 2022). The transcription factor *GATA3*, presumably associated with cochlear identity, is instead expressed at low levels in a small number of HC, but is present in OEP cells, matching our histological characterization (Fig. S10B). Within the OEP subcluster, we detected expression of *USH1C*, *SPARCL1*, *CLDN14* and *COL9A2*. *MEIS2*, previously described in vestibular epithelia, and *TECTA*, identified in cochlear epithelia (Wilkerson et al., 2021), are also expressed. Overall, the maturity of the IEO-derived HC and supporting cells at day 60 of *in vitro* differentiation corresponds to week 10-12 human fetal development. We were not, however, able to provide a clear distinction of vestibular or cochlear identity at this stage.

DISCUSSION

Benchmarking human iPSC-derived IEOs

The restricted access to human inner ear tissue is a primary limiting factor in studying its development and validating therapeutic strategies for hearing and balance restoration (Roccio, 2021). In this respect, stem cell-based models, such as the IEOs described here, offer a promising alternative to this problem. In contrast to models which rely on human somatic cells (Chen et al., 2007; Roccio et al., 2018; Senn et al., 2019; Taylor et al., 2015) or trans-differentiation strategies (Costa et al., 2015; Menendez et al., 2020; Noda et al., 2018), the use of pluripotent cells as a starting point enables the study of early otic developmental stages. Furthermore, by generating complex sensory units, including sensory and non-SE, neurons and surrounding otic mesenchyme, IEOs offer a platform to study more complex aspects of organ physiology and pathology compared with monotypic cultures.

Here, we have evaluated in detail a previously reported protocol to guide iPSCs through consecutive steps of otic development (Koehler et al., 2017; Nie and Hashino, 2020) and compared, for the first time, the *in vitro*-derived otic tissue with early human embryos. This represents a first step towards the benchmarking of IEOs. Similar studies have been performed with brain organoids (Camp et al., 2015; Pollen et al., 2019), retinal organoids (Cowan et al., 2020; Wahle et al., 2023) and pancreatic organoids (Goncalves et al., 2021) to name a few examples, with the complementary goal to create developmental human cell atlases (Haniffa et al., 2021). IEOs are a relatively new addition to the catalogue of *in vitro*-derived organ models. Our work, together with other recent studies, aims at providing a robust foundation for broader application of IEOs (Moore et al., 2022; Steinhart et al., 2023; van der Valk et al., 2023).

Although we provide a comparison using immunostaining of tissue sections, we have not been able to obtain and to process freshly isolated tissue from early embryos (CS11-13) for a comparative gene expression analysis using scRNA-seq. This remains a limitation of this study and potentially a roadblock for similar endeavors. Not only given the difficulty in obtaining these early samples, but also due to the small number of cells forming the OV at this stage, making their identification in unsorted single-cell embryo datasets very hard or impossible (Xu et al., 2023).

BMP signaling in placode development

The IEO protocol was developed with the goal to recapitulate otic development *in vitro* using consecutive addition of small molecules and growth factors (Koehler et al., 2013, 2017). We have characterized three major stages of the induction protocol: placode differentiation, otic vesicle formation and, finally, SE maturation.

The first step is triggered in iPSC aggregates cultured in the presence of Matrigel and a TGFβ inhibitor, by exposure to low

Development (2023) 150, dev201865. doi:10.1242/dev.201865

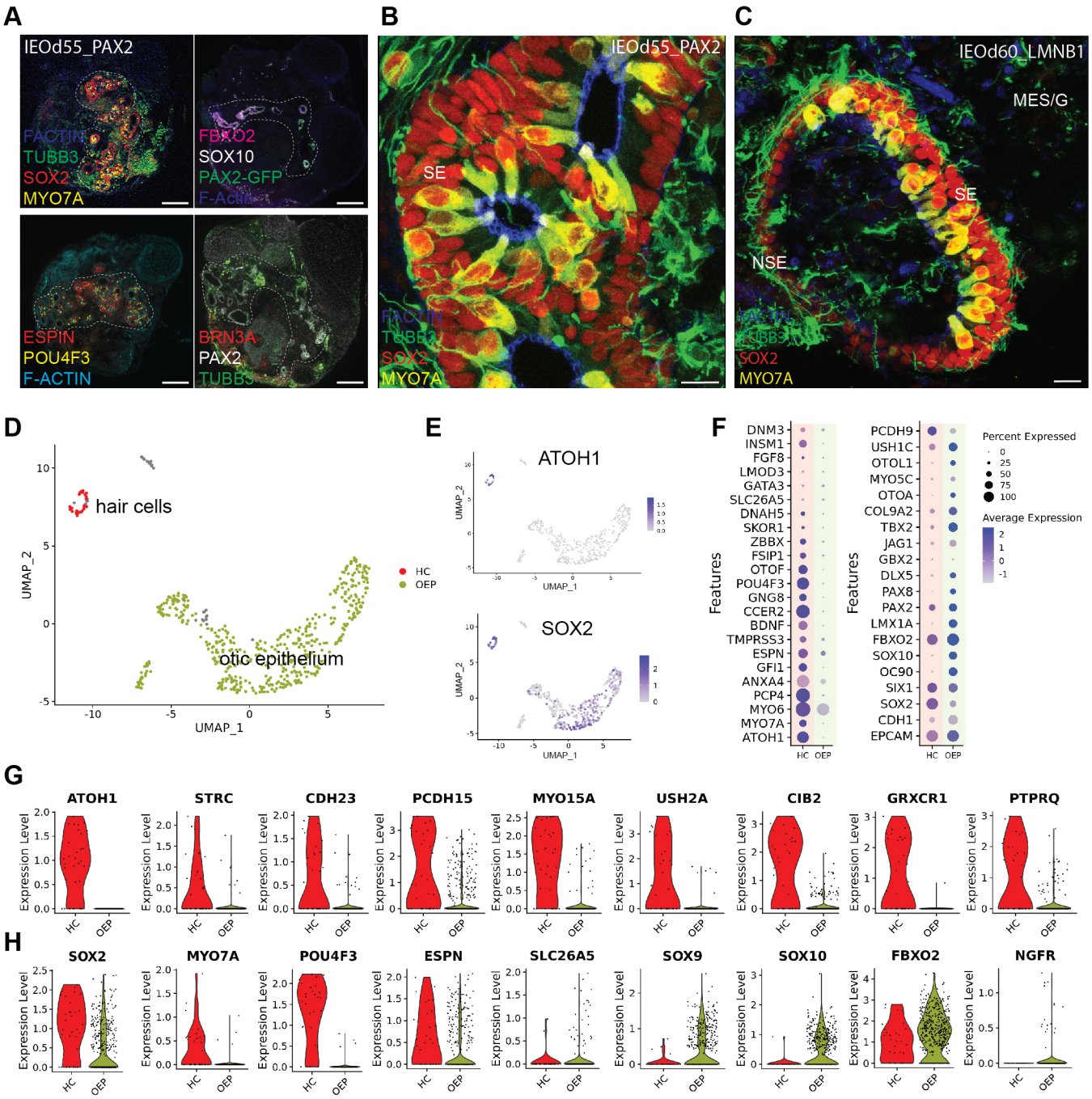


Fig. 6. Characterization of sensory epithelia in IEOs at days 55 and 60. (A) Characterization of IEO at day 55 of differentiation (PAX2-GFP iPSC line). Different sections of the same organoids are shown. Otic marker-positive areas are contoured with white-dashed line. (B,C) Sensory vesicle derived from the PAX2-GFP iPSC line (day 55; IEOd55) and LMNB1-RFP iPSC line (day 60; IEOd60) (C). Staining for MYO7A, SOX2, TUBB3 and F-Actin are shown. MES/G, mesenchyme/glia; NSE, non-sensory epithelium; SE, sensory epithelium. (D) UMAP plot of the selected OEP (green) and HC (red) clusters. (E) UMAP plots of the selected cells showing *ATOH1* and *SOX2* expression. (F) Dot plot with relative expression of known marker genes in the selected OEP and HC cluster. (G,H) Violin plots showing expression levels of selected genes in HC and OEP. Scale bars: 100 µm (A); 10 µm (B,C).

levels of FGF2 and BMP4. BMP is a potent inhibitor of neural fate and plays a crucial role for ectoderm differentiation towards non-neural fate (Wilson and Hemmati-Brivanlou, 1995). In the first 4 days of culture, BMP4 triggers the differentiation of NNE and PE on the surface of the iPSC aggregates. BMP signaling is subsequently inhibited, and high levels of FGF2 and WNT signaling are used to promote OP fate (Martin and Groves, 2006; Zelarayan et al., 2007). Optimization of the BMP4 level is a crucial factor for successful placodal induction in IEOs in all the iPSC lines tested here. This requires fine tuning for each line, to account for endogenous morphogen production. In some lines (Koehler et al., 2017; Nie et al., 2022), or other studies using 2D approaches (Dincer et al., 2013; Ealy et al., 2016), no exogenous BMP was used to promote placodal fate. Experiments performed with hESCs on micropatterns point to co-integration of BMP and WNT signaling to induce placode differentiation (Britton et al., 2019). In the presence

Development (2023) 150, dev201865. doi:10.1242/dev.201865

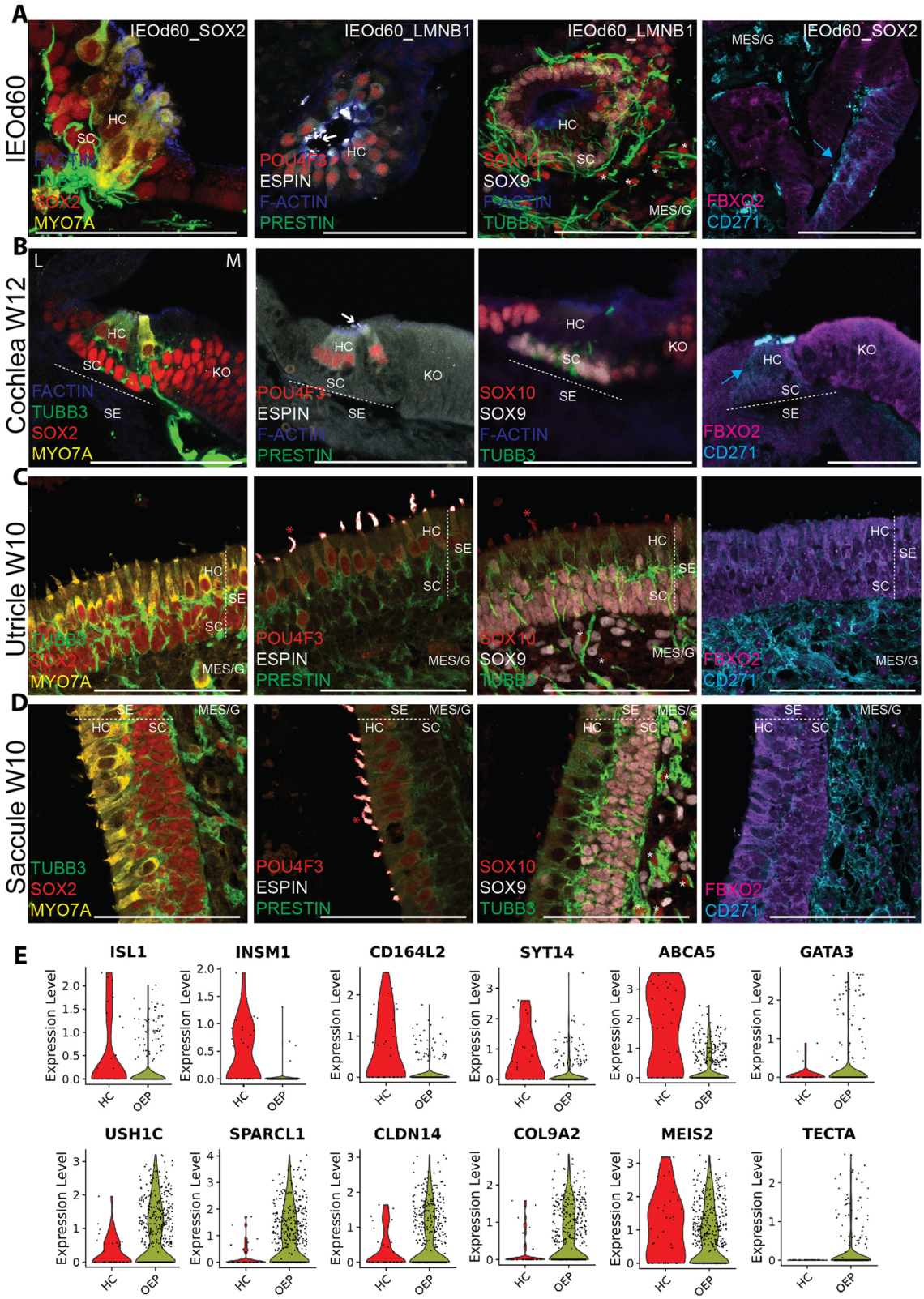


Fig. 7. Comparison of organoid marker expression and human fetal cochlea, utricle and saccule. (A) Representative images of IEO-derived sensory vesicles from two different cell lines (SOX2-GFP iPSC and LMNB1-RFP iPSC) at day 60 of differentiation. (B) Cochlea sections at week 12 of development (sample E1291). (C) Utricle sections at week 10 of development (sample EF1). (D) Saccule sections at week 10 of development (sample EF1). HC, hair cells; KO, Kölliker's organ; MES/G, mesenchyme/glia; SC, supporting cells; SE, sensory epithelium. Single channels of the images are shown in Fig. S9, including extended figure legend. Red asterisks (C,D) indicate cross-reactivity of the goat anti mouse IgG1 antibody with hair bundles (used for POU4F3 and SOX10 staining). This has been detected only on paraffin-embedded sections. White asterisks (A,C,D) show SOX10^{+} glia cells. White arrows (A,B) indicate espin-positive immature hair bundles. Blue arrows (A,B) indicate NGFR^{+} otic epithelia. Dashed white lines indicate sensory epithelia (SE). (E) Violin plots showing expression levels in HC and OEP for selected genes. Scale bars: 100 µm.

Development (2023) 150, dev201865. doi:10.1242/dev.201865

of BMP, WNT signaling favored the co-development of NC from ectodermal progenitors. Inhibition of WNT with the inhibitor IWP2, on the other hand, enhanced placodal fate, even with low BMP4 supplementation. The co-development of NC and placode in IEO suggests the presence of endogenously secreted WNTs, and possibly BMP. This agrees with the extensive NC differentiation observed in the absence of added BMP4 (Fig. S2).

Co-differentiation of NC and NC-derived mesenchyme, even though considered 'off-target', may provide the proper context for subsequent morphogenetic events leading to otic vesicle formation *in vitro*. We compared IEOs at the placode induction stage (day 8-12) with human samples at CS11 (day 24-25). Even though not perfectly matching in terms of developmental time points, most of the placodal markers were conserved and similarly expressed. PAX2, already expressed *in vivo* in the invaginating OP, was not detected in organoids at day 8 but appeared in IEOs starting at day 20.

Otic epithelia and neuroblast differentiation

The second stage we characterized spans between day 20 and day 40 of *in vitro* differentiation, during which OE and neuroblasts arise. Both cell types were indeed identified in the day 26 RNA-seq dataset. IEO-derived OE and neuroblasts express markers previously found in the developing murine otocysts (Durruthy-Durruthy et al., 2014; Hartman et al., 2015), and based on our histological characterization match the CS13 stage of development.

Our characterization of IEO-derived OE corroborates recently reported findings (Nie et al., 2022). IEO-neuroblasts, besides general undifferentiated markers, express genes such as *CASZ1*, *EPHA5* and *SHOX2* and lack expression of *SALL3*, matching the pattern recently reported in the developing cochlear ganglion (Sun et al., 2022). Furthermore, they lack expression of geniculate ganglion neuron genes such as *PHOX2B, PHOX2A* and *NEUROG2*, suggesting that these neuroblasts may resemble SGN precursors.

In this study we did not assess whether these ONB eventually developed into SGNs. Our analysis at later time points focused on the SE components. The neuronal population identified at day 60 (Fig. S8), after EPCAM sort, may represent only a fraction of less differentiated cells. We have therefore not analyzed it in detail. Transcriptional profiling of whole organoids is starting to shed light on the neuronal populations derived in IEOs (Steinhart et al., 2023). Nevertheless, in the absence of a complete transcriptional atlas for cranial ganglia, DRGs and concomitant analysis of CNS neurons, we feel it is currently not possible to assign identity to these populations unequivocally.

Hair cell maturation

In vivo differentiation and maturation of HC in the inner ear sensory patches is not synchronous and it happens over the course of a few weeks in humans. HC in the vestibular organs develop before HC in the cochlea (~2 weeks). Cells at the base of the cochlea develop before cells in the apical turn, and inner hair cells (IHC) differentiate before OHC. The whole process spans between weeks 8 and 13 (Locher et al., 2013; Roccio et al., 2018).

Our comparison between IEO-derived sensory vesicles at day 60 *in vitro* and the human inner ear shows a similar marker expression as for the fetal cochlea at week 12 and the human fetal utricle and saccule at week 10. This is the case both for HC and supporting cell markers.

Our transcriptomic data shows that the HC derived by day 60 *in vitro* express 'general' HC markers. At this time point, the gene signature defining subclasses of HC (cochlear versus vestibular) is not yet clear. We found, in fact, genes previously associated with both types of SE. This could indicate that both types differentiate but, given the timing, a more substantial number of vestibular HC would be present at early stages. Alternatively, the cues provided for otic induction, in particular WNT activation, may be skewing the culture to dorsal/vestibular fate. Recent work exploiting scRNA-seq to characterize HC from wild-type or CDH7-mutant iPSC lines, suggest that the majority of cells derived *in vitro* after 70 days have a vestibular signature (Nie et al., 2022). Additional activation of SHH signaling and inhibition of WNT during otic vesicle maturation appears to promote cochlear fate. However, this only becomes apparent in long term cultures >140 days (Moore et al., 2022).

Although the number of studies focused on the molecular characterization of inner ear SE has increased with the advent of single cell genomics (Burns et al., 2015; Li et al., 2018; Nie et al., 2022; Petitpre et al., 2022; Ranum et al., 2019; Sun et al., 2022; Waldhaus et al., 2015; Wilkerson et al., 2021), a comprehensive and simultaneous comparison of the different SE and neurons, across developmental stages, is currently lacking. The specificity and selectivity of many genes used as 'markers' to each organ, and in particular for human tissues, is not yet robustly established.

GATA3 for example, is initially broadly expressed in the otocyst and then acts as key regulator of SGN and cochlear prosensory domain maturation in the mouse (Luo et al., 2013). Although GATA3 has been identified in many studies as enriched in the cochlea (Cai et al., 2015; Elkon et al., 2015; Scheffer et al., 2015; Wilkerson et al., 2021) it has been observed also in the vestibular epithelia in the human cochlea (Johnson Chacko et al., 2020). Here, we found low levels of GATA3 expression in a few HC. High *GATA3* expression was found instead in a subset of the OEP cells. These co-express *GATA2*, *BMP4*, *GJB2*, *GJB6* and *ISL1*. This cluster appears to match the gene expression of non-sensory cochlear floor regions (lateral domain), but both a higher number of cells and better references for cochlear and vestibular epithelia would be needed to conclude about the true nature of these cell types.

Strengths and limitations of IEO characterization by scRNA-seq

The use of a high number of 'unselected' and unsorted organoids for scRNA-seq is in principle an ideal tool to obtain an unbiased representation of the global efficiency of the induction protocol (Steinhart et al., 2023; van der Valk et al., 2023). Nevertheless, less abundant cell types can be missed with this approach. Sorting strategies may allow us to circumvent this issue.

At the placodal stage (day 8 of differentiation) posterior placodal cells represented 21% of total cells in this study. PE is localized at the external layer of the aggregates. It is therefore possible that the relative percentage of these cells may be limited by the aggregate size. In a subsequent step we have identified 4-5% of cells differentiating to OE and an additional 0.7% of cells representing otic neuroblasts. At this step, we relied on EPCAM expression and FACS sorting to enrich for otic progenitors. However, we did not collect the negative fractions, limiting our assessment of the full cellular composition of the organoids at this stage.

Our analysis at later time points (day 60), resulted in the identification of a small population of HC; however, by our estimation, the number of HC in our transcriptomic data set is inferior to what we observed in the histological analysis of the organoids. We suspect this may be due to problems triturating organoids to single cells, especially the compact epithelia we

Development (2023) 150, dev201865. doi:10.1242/dev.201865

observed at day 60. Cell preparation methods are known to introduce biases in the abundancy of different cellular populations (Denisenko et al., 2020; Uniken Venema et al., 2022). In the absence of fluorescent reporters marking HC, the isolation of this specific population is hard to optimize. Fluorescent reporter lines for HC, supporting cells or neuroblasts, or additional surface markers to purify and enrich for low-abundance cells, should provide better coverage of these cell types in future studies.

Outlook and conclusions

This study provides the first unique molecular analysis of otocyst development in human embryos, serving as a reference for further developmental studies. We demonstrate that the current state-of-the-art IEO protocol generates cell types that match, in terms of marker expression, human otic progenitors and follow similar developmental timings as the *in vivo* counterpart. IEOs could, therefore, significantly contribute to informing human otic development. Alternative strategies, possibly deviating from the developmental trajectory, may allow for further enrichment of the cells of interest at the expense of other tissues (Dincer et al., 2013; Qi et al., 2017).

Some level of variability nevertheless remains in IEO generation and final SE maturation. Optimizing culture conditions, for example, using bioreactors or automated systems for medium exchange may eventually enable standardization and further enhance reproducibility for generating functionally mature cell types. The current model consists of closed vesicles or tubules that may not experience the same degree of fluid-induced shear stress, nor vibration-induced maturation that the inner ear experiences. The lack of these mechanical cues could limit the proper maturation of the different cell types. One could speculate that more advanced culture systems, such as organs-on-a-chip, may provide models to dissect the contribution of different factors to cell maturation.

MATERIALS AND METHODS

Human fetal sample collection

Human samples were collected in two different medical centers. Procurement and procedures were performed with full approval by the respective Ethics Committee. All experiments were performed in accordance with guidelines enunciated in the Declaration of Helsinki and the guidelines of the International Society For Stem Cell Research. Samples E1026, E1027, E1037, E852, E1291, E1203 and E1201 were collected as previously described (Roccio et al., 2018). Signed informed consent of the donors for procurement of the aborted embryos/fetuses and for use of tissues in research was obtained. Procedures were performed with full approval by the Ethics Committee of the Medical Faculty of the University of Bern and the Ethics Committee of the State Bern, Switzerland (Gesundheits-und Fürsorgedirektion des Kantons Bern, Kantonale Ethikkommission für die Forschung (Project ID: 2016–00033/KEK-Nr. 181/ 07). Tissues were collected the same day, as early as possible after the procedure, otherwise discarded. Samples were then anonymized. Staging was performed by comparing tissue morphology to atlases (de Bakker et al., 2016) or as previously described (Evtouchenko et al., 1996; Roccio et al., 2018). The sample EF1 was collected at the Leiden University Medical Center (LUMC), The Netherlands, according to Dutch legislation (Fetal Tissue Act, 2001) under the protocol number B19.070 approved by the Medical Research Ethics Committee of LUMC as well as written informed consent of the donor following the Guidelines on the Provision of Fetal Tissue set by the Dutch Ministry of Health, Welfare, and Sport (revised version, 2018). The inner ear tissue was collected after elective termination of pregnancy by vacuum aspiration. Fetal age was determined by obstetric ultrasonography before termination, with a standard error of 2 days. All references to human developmental weeks refer to fetal age.

After collection, samples were fixed overnight in paraformaldehyde (PFA), in PBS (pH 7.4) (11762.00250, Morphisto) at 4°C and subsequently placed in PBS (14190169, Thermo Fisher Scientific/Life Technologies) and processed for immunostaining as indicated below.

iPSC lines and culture

Cell lines (human iPSC SOX2-GFP and human iPSC LMNB1-RFP) derived from the parental WTC-11 human iPSC were obtained from the Coriell Institute (NJ, USA) and generated at the Allen Institute for Cell Science (WA, USA) at passage 29 frozen in mTeSR™ Plus medium (STEMCELL Technologies). The PAX2-EGFP-iPSC line was generated starting from BJS iPSC lines at the Harvard Stem Cell Institute (HSCI; MA, USA) core facility. BJ fibroblasts (ATCC) were reprogrammed to generate iPSC. Knock-in was performed using CRISPR-Cas9 (cell line generation: M. Petrillo, H. Lahlou, S. Heller, M. Ealy, A. Müller, H. Löwenheim; M.R., A.E., unpublished). Clone C2 with bi-allelic insertion was used for the experiments given the brighter GFP fluorescence. Cells were obtained at passage 34, frozen in mTESR1 medium. Cells were thawed according to the provider's protocol and the medium was gradually changed to Essential 8 Flex Medium (E8f) (A2858501, Thermo Fisher Scientific/Life Technologies) supplemented with 100 µg/ml Normocin (4069-ant-nr-1, InvivoGen), on recombinant human vitronectin (A14700, Thermo Fisher Scientific/Life Technologies)-coated six-well plates. Each well was coated in 1 ml PBS containing 0.5 mg/ml vitronectin for at least 1 h at 37°C before cell seeding. Cells were passaged at ∼70-80% confluency or every 4 or 5 days using Accutase (7002353, Thermo Fisher Scientific/Life Technologies). Briefly, the medium was removed, cells were rinsed with PBS and incubated for 4-5 min with 500 µl Accutase at 37°C. Then 1 ml of the medium was added to the plates for cell dissociation and cells were quickly centrifuged (300 ***g***, 5 min). The cell pellet was resuspended in E8f with 10 µM ROCKi (Y-27632, ALX-270-333-M005, EnzoLifeSciences) and replated. The next day the medium was changed to remove the ROCKi, and subsequently changed according to medium manufacturer's instructions.

Cell were authenticated by the provider and tested for contamination with *Mycoplasma* by regular PCR testing (Microsart, Sartorius). iPSC lines were analyzed at thawing for expression of pluripotency markers SOX2, OCT4, NANOG, TRA1-60 and reporter expression (Fig. S11). Cells obtained from the Coriell Institute at passage 29 were used between passages 30-35. Cells obtained from the HSCI core facility at passage 34 were used between passages 35-40.

IEO differentiation

iPSC differentiation to IEO followed previously described protocols (Koehler et al., 2017; Nie and Hashino, 2020) with some modification. Briefly, 70-80% confluent iPSC cultures were dissociated to a single cell suspension in E8f supplemented with 20µM ROCKi. Then 3500 cells per well were aggregated in round bottom low-binding 96-well plates (174929, Thermo Fisher Scientific/Life Technologies) by centrifugation (100 ***g***, 6 min) in 100 µl E8f medium with 20 µM ROCKi. The following day, the addition of 100 µl E8f was used to dilute the ROCKi to 10 µM.

On day 2 of culture (day 0 differentiation) the organoids, ∼500 µm in diameter, were collected, rinsed twice in E6 medium (A1516401, Thermo Fisher Scientific/Life Technologies) and subsequently transferred to differentiation medium 'E6/SB/F/B4' (see below) with one organoid/100 µl differentiation medium/well in new round-bottom low-binding plates.

Differentiation medium E6/SB/F/B4 consisted of E6 supplemented with 2% growth factors-reduced Matrigel (354230, Corning), SB-431542 at 10 µM (CAY13031, Cayman Chemical), 4 ng/ml FGF2 (SRP3043, Merk/Sigma-Aldrich) and BMP4 (314-BP-010, Biotechne/R&D Systems) from 0.5-10 ng/ml. The optimal concentration for placode induction with the cell line used ranged from 1.5-2.5 ng/ml. On days 3-4 of differentiation, FGF2 and LDN193189 (CAY19396, Cayman Chemical) were added to the medium at the final concentration of 50 ng/ml and 200 nM, respectively. On day 8, the medium was supplemented with 3 µM CHIR99021 (361571 Avantor/WVR) to promote otic fate. CHIR99021 was further supplemented on day 10. On day 12 of *in vitro* culture, the organoids were

Development (2023) 150, dev201865. doi:10.1242/dev.201865

transferred to Organoid Maturation Medium (OMM) consisting of 1:1 Neurobasal (21103049, Thermo Fisher Scientific/Life Technologies), Advanced-DMEMF12 (12634028, Thermo Fisher Scientific/Life Technologies) supplemented with 0.5× B27 (12587010, Thermo Fisher Scientific/Life Technologies), 0.5× N2 (17502048, Thermo Fisher Scientific/Life Technologies), 1× Glutamax (35050061, Thermo Fisher Scientific/Life Technologies), 1× β-mercaptoethanol (21985023, Gibco/Thermo Fisher Scientific/Life Technologies) and CHIR99021 3 µM.

Organoids were transferred at one organoid per well in 24-well plates (non-treated; 144530 Thermo Fisher Scientific/Life Technologies) pre-coated as follows: 500 µl anti-adherent solution (STEMCELL Technologies) was added to each well for 5 min at room temperature, the surfactant was then removed by aspiration, and wells were washed twice with 1 ml PBS and dried for 5 min before use.

The medium was refreshed to provide fresh CHIR on day 15 of differentiation. From day 18 onwards, half of the OMM medium was changed every 2 days and refreshed with OMM without Matrigel. Samples were collected at selected time points and either fixed for characterization or dissociated to single cells for flow cytometry/scRNA-seq.

Organoid and embryo characterization

Cryosections

Organoids were collected using wide-opening pipet tips at different time points and fixed in 4% PFA in PBS (pH 7.4) for 15 min at room temperature, then rinsed in PBS and incubated for 24 h in 18% sucrose (S0389, Sigma-Aldrich) solution at 4°C and transferred for another 24 h in 30% sucrose in PBS. Organoids were then transferred to OCT medium (361603E, Avantor/VWR) in cryomolds and frozen on a dry-ice bed. Cryoblocks were incubated at for at least 1 day at −80°C before sectioning.

The same procedure was used for human samples (CS11-13). Given the scarcity of the embryonic tissue (n=1 embryo per developmental time point), consecutive cryosections were collected on different slides, on which we performed immunostaining for 3-4 marker combinations. The images displayed in Fig. 2 are consecutive sections to the ones displayed in Fig. 1. To improve clarity, some stainings are shown as separate channels (e.g. Fig. S1E, Fig. S7D, Fig. S9), this is indicated in the figure legends. For the W12 cochleae, these were decalcified with 0.5 M EDTA (15575020 Thermo Fisher Scientific/Life Technologies) in PBS for 30 days before preparation for cutting as cryosections.

Cryoblocks were sectioned at a thickness of 12 µm with a Cryostat (Leica CM3050 S) and sections were collected on Superfrost Plus Adhesion microscope slides (J1800AMNZ, Epredia). For experiments where organoids were exposed to different conditions during the differentiation phase, all conditions were collected on the same glass slide for further comparison with antibody-based staining.

Paraffin embedding end sectioning

Samples embedding in paraffin was performed as follows: after fixation samples were dehydrated in an increasing ethanol series (70%-99%; 84050068.2500, Boom), cleared in xylene (534056, Honeywell) and embedded in paraffin wax (2079, Klinipath). Sections of 4-5 µm were cut using a rotary microtome (HM355S, Thermo Fisher Scientific). Sections were deparaffinized in xylene and rehydrated in a descending series of ethanol (96%-50%) and several rinses in deionized water. Before immunostaining, antigen retrieval was performed in 10 mM sodium citrate buffer (pH 6.0; S1804-500G, Sigma-Aldrich) for 12 min in a microwave at ∼97°C.

Imaging and image analysis

Samples were permeabilized with PBS containing 0.1% Triton X-100 (X100, Sigma-Aldrich) and subsequently incubated with blocking buffer (BB) containing 2% bovine serum albumin (BSA; A2153, Sigma-Aldrich) and 0.01% Triton X-100 in PBS for 2 h at room temperature. Finally, each slide was incubated with 250 µl of antibody-containing solution in BB. The antibodies used are shown in Table S1. After primary antibody incubation (overnight at 4°C or 2 h at room temperature), samples were rinsed three times for 10 min with PBS and incubated with Alexa-Fluor conjugated antibodies (Table S1) (overnight at 4°C or 2 h at room temperature). Finally, slides were washed with PBS and mounted using glycerol mounting medium with DABCO (INTFP-WU1420, Interchim).

Image acquisition and quantification

Widefield images were acquired using a Zeiss Axio-observer Z1 microscope with a motorized stage. Filter sets were as follows: DAPI (ex: BP390/22-25; em: BP455/50), GFP (ex: BP484/25; em: BP525/50), DsRed (ex: BM553/18; em: BM607/70), CY5 (ex: BP631/22; em: BP690/50). For organoid assessment, different experimental conditions (or time points) were positioned on the same glass slides (see also Fig. S4A). Tile scans were acquired for comparative assessment of marker expression. Single images of organoids/sections were then acquired using 10× (EC Plan Neufluar) or 20× (LD Plan Neufluar) objectives.

Areas of interest were marked and re-imaged using a laser-scanning confocal microscope. Confocal images were acquired using a Leica SP8 microscope either with a 10× (HC PL Fluotar) air objective; a 20× (PL APO CS) air objective or a 63× (HC PL APO CS2 NA 1.4) oil objective. Sequential imaging was used to acquire different channels.

To assess marker-positive areas, image files were opened using FIJI (Schindelin et al., 2012). The contour of the organoids was drawn manually on the DAPI channel and used to quantify the organoid area. Within this ROI, a fluorescent threshold was placed – on the channel of the marker of interest – to identify signal-positive areas. Alternatively, the vesicle contour was manually selected and the lumen volume subtracted. For organoids containing multiple vesicles, the sum of all areas of each vesicle was calculated and expressed as a ratio to the area of the organoid section. We analyzed 2-3 images of the same organoids and 3-4 organoids per condition. If confocal images with multiple stacks were acquired, images are shown as a 3D projection stack.

Organoid dissociation for scRNA-seq

Organoids were collected at the defined time points in a 15 ml falcon tube and allowed to sediment by gravity. After removing the culture medium, organoids were incubated with Accutase (1×) and DNAse1 0.5 mg/ml (10104159001, Sigma-Aldrich) for 25-30 min at 37°C in a water bath, in 1 ml dissociation solution per plate (at day 8) or per half plate (>day 18). Every 5 min, organoids were triturated mechanically by pipetting with p1000 pipet tips ten times. After 25-30 min, cells were washed with medium containing 10 µM ROCKi and centrifuged for 5 min at 300 ***g***. The pellet was then resuspended in PBS containing 2% BSA and 10 µM ROCKi and passed through a cell strainer with 40 µm pore size (352235, Corning) to eliminate clumps. Cells were then centrifuged again (5 min at 300 ***g***) and resuspended in 550 µl PBS containing 2% BSA and 10 µM ROCKi on ice.

Single-cells isolated from day 8 organoids (200 unselected organoids) were incubated for 5 min at room temperature with Calcein-AM (C3099, Thermo Fisher Scientific/Life Technologies) and subsequently sorted on a FACS Aria (BD Biosciences) to exclude debris, doublets and isolate single positive (live) cells (these represented 96% of the cell suspension). Single cells from day 26 organoids (140 unselected organoids) were incubated on ice for 45 min with 40 µl of an EPCAM-Pe-Cy7 antibody (25-9326, eBioscience/Thermo Fisher Scientific; 0.36 µg antibody in 500 µl buffer). After washing, cells were sorted on a FACS Aria to purify Pe-Cy7^{+} cells. Debris and doublets were also excluded. Day 60 organoids [48 unselected organoids (experiment 1) or eight selected organoids (experiment 2)] were triturated as above and incubated for 30 min with 10 µl (0.12 µg) EPCAM-Pe-Cy7 antibody/1×10^{6} cells in 500 µl buffer. After washing, cells were sorted on a FACS Aria to purify Pe-CY7^{+} cells. Unstained controls were used to define the gating strategy. The selection of organoids for experiment 2 was performed by live imaging of GFP fluorescence (SOX2-GFP) and brightfield imaging to visualize vesicles. Only organoids with visible vesicles were used. An example of such organoids is shown in Fig. S8C.

After sorting, cells were centrifuged for 10 min at 300 ***g*** to remove FACS fluids and resuspended in a 0.04% BSA in PBS buffer at the concentration of 1000 cells/µl and placed on ice before loading on the 10x Chromium according to the manufacturer's instruction. Sorting was performed at the Flowcytometry Facility of the University of Zurich, Switzerland.

Development (2023) 150, dev201865. doi:10.1242/dev.201865

scRNA-seq and data analysis

The quality and concentration of the single-cell preparations were evaluated using a hemocytometer in a Leica DM IL LED microscope and adjusted to 400 cells/µl. We loaded 17,200 cells per sample into the 10x Chromium controller and library preparation was performed according to the manufacturer's indications (Chromium Next GEM Single Cell 3′ Reagent Kits v3.1 protocol). The resulting libraries were sequenced in an Illumina NovaSeq sequencer according to 10x Genomics recommendations (paired-end reads, R1=28, i7=10, i5=10, R2=90) to a depth of around 40,000 reads per cell. scRNA-seq reads were processed with 'cellranger count' v6.1.2. to generate the single-cell gene expression matrix. Subsequently, we filtered doublet cells using the R/Bioconductor package 'scDblFinder' (Germain et al., 2021), and we removed low-quality cells using the quality metrics computed by the package 'scater' (McCarthy et al., 2017). The remaining cells were analyzed using the Seurat package (Hao et al., 2021). The workflow included normalization, dimension reduction and clustering, as well as the identification of marker genes for clusters and differentially expressed genes. Additional details for the analysis can be found in Table S2. In the Seurat processing, with respect to all other parameters, we used the default settings.

Datasets at day 60 of differentiation obtained from two independent experiments were integrated using the Seurat 'IntegrateData' as previously described (https://satijalab.org/seurat/articles/integration_introduction.html; Hao et al., 2021). Selection of the population of interest (OEP and HC) was performed based on marker gene expression (https://satijalab.org/seurat/reference/addmodulescore). Modules including OEP genes and HC genes (Table S3) were used to select and further re-cluster these cell populations. Data processing and analysis were performed using the Sushi platform (Hatakeyama et al., 2016).

Data are visualized either as Uniform Manifold Approximation and Projection (UMAP) plots or as violin plots of normalized data. Sequencing and bioinformatic analysis were performed at the Functional Genomics Center Zurich, Switzerland.

Statistical analysis and reproducibility

The experiments described here have been performed with three iPSC lines. We include the data from ∼25 independent experiments, used for different time points or type of analysis. The number of biological replicates is indicated in the text and/or figure legends. Data are mean±s.d. Statistical significance across conditions (Fig. 5J; Fig. S2B,C) has been tested with one way ANOVA with multiple comparison (GraphPad Prism v9.5.1).

Acknowledgements

We thank the staff of the Flow cytometry core facility of the University of Zurich (Dr Mario Wickert, Dr Tatiane Gorski and Dr Philip Schätzle) for their professional help and flexibility with sorting experiments. We thank the staff of the Genomic core facility, in particular Dr Daniel Ehrsam and Dr Qin Zhang for their help with sample preparation. In addition, we thank Edward van Beelen, from the Otobiology Lab, LUMC, for fetal specimen collection, Prof. Dr Christian Grimm from the Department of Ophthalmology, USZ, for access to the cryostat and Dr Melanie Generali, from the iPSC core facility of the University of Zurich and IREM institute, for help with iPSC cultivation. Image acquisition was performed using microscopes of the imaging core facility of the University of Zurich. The human PAX2-GFP iPSC line was generated within a previous EU-FP7-funded project (www.otostem.org). We thank Prof. Dr Hubert Löwenheim and all the consortium members for sharing the line. We thank Dr Bernadette de Bakker from the Amsterdam UMC for allowing the reprint of images from the 3D Embryo Atlas (https://www.3dembryoatlas.com).

Competing interests

K.R.K. is an inventor on patents related to the inner ear organoid system and consults for STEMCELL Technologies on matters related to the technology. The other authors declare no competing interests.

Author contributions

Conceptualization: M.R.; Methodology: D.D., S.A.J., H.R., J.F.C., J.Z., K.R.K.; Software: H.R., J.F.C.; Validation: D.D., S.A.J., K.R.K.; Formal analysis: D.D., S.A.J., H.R., J.F.C., V.V., M.R.; Investigation: D.D., S.A.J., V.V., S.D.S., H.R.W., A.E., H.L., W.H.v.d.V., M.R.; Resources: H.R., J.F.C., S.D.S., H.R.W., A.E., H.L., W.H.v.d.V.; Data curation: S.A.J., H.R., J.F.C., M.R.; Writing - original draft: S.A.J., M.R.; Writing - review & editing: H.L., W.H.v.d.V., J.Z., K.R.K., M.R.; Visualization: H.R., J.F.C., M.R.; Supervision: M.R.; Project administration: M.R.; Funding acquisition: H.L., K.R.K., M.R.

Funding

The project was sponsored by the Zürcher Stiftung für das Hören, the Vontobel-Stiftung, the Schmieder Bohrisch Stiftung, Jubiläumsstiftung von Swiss Life, the Novartis Stiftung für Medizinisch-Biologische Forschung (grant 22B133), the Royal National Institute for Deaf People (grant 007) to M.R., 'la Caixa' Foundation (Fellowship 100010434, CF/BQ/EU21/11890066 to J.F.C.), the Hearing Restoration Programme (U.S. Department of Defense; grant W81xWH211810 to K.R.K. and M.R.), the National Institutes of Health (grant R01DC017461 to K.R.K.) and the Novo Nordisk Foundation (grant NNF21CC0073729 to H.L.). Deposited in PMC for release after 12 months.

Data availability

The single cell sequencing data generated by this study and presented in the publication have been deposited in the NCBI Gene Expression Omnibus (Edgar et al., 2002) and are accessible through accession number GSE229148.

Peer review history

The peer review history is available online at https://journals.biologists.com/dev/lookup/doi/10.1242/dev.201865.reviewer-comments.pdf

References

Adameyko, I., Lallemend, F., Furlan, A., Zinin, N., Aranda, S., Kitambi, S. S., Blanchart, A., Favaro, R., Nicolis, S., Lubke, M. et al. (2012). Sox2 and Mitf cross-regulatory interactions consolidate progenitor and melanocyte lineages in the cranial neural crest. *Development* **139**, 397-410. doi:10.1242/dev.065581

Alsina, B. and Whitfield, T. T. (2017). Sculpting the labyrinth: morphogenesis of the developing inner ear. *Semin. Cell Dev. Biol.* **65**, 47-59. doi:10.1016/j.semcdb.2016.09.015

Appler, J. M. and Goodrich, L. V. (2011). Connecting the ear to the brain: molecular mechanisms of auditory circuit assembly. *Prog. Neurobiol.* **93**, 488-508. doi:10.1016/j.pneurobio.2011.01.004

Baker, C. V., Stark, M. R., Marcelle, C. and Bronner-Fraser, M. (1999). Competence, specification and induction of Pax-3 in the trigeminal placode. *Development* **126**, 147-156. doi:10.1242/dev.126.1.147

Bok, J., Dolson, D. K., Hill, P., Ruther, U., Epstein, D. J. and Wu, D. K. (2007). Opposing gradients of Gli repressor and activators mediate Shh signaling along the dorsoventral axis of the inner ear. *Development* **134**, 1713-1722. doi:10.1242/dev.000760

Bouchard, M., De Caprona, D., Busslinger, M., Xu, P. and Fritzsch, B. (2010). Pax2 and Pax8 cooperate in mouse inner ear morphogenesis and innervation. *BMC Dev. Biol.* **10**, 89. doi:10.1186/1471-213X-10-89

Britton, G., Heemskerk, I., Hodge, R., Qutub, A. A. and Warmflash, A. (2019). A novel self-organizing embryonic stem cell system reveals signaling logic underlying the patterning of human ectoderm. *Development* **146**, dev179093. doi:10.1242/dev.179093

Burns, J. C., Kelly, M. C., Hoa, M., Morell, R. J. and Kelley, M. W. (2015). Single-cell RNA-Seq resolves cellular complexity in sensory organs from the neonatal inner ear. *Nat. Commun.* **6**, 8557. doi:10.1038/ncomms9557

Cable, J., Barkway, C. and Steel, K. P. (1992). Characteristics of stria vascularis melanocytes of viable dominant spotting (Wv/Wv) mouse mutants. *Hear. Res.* **64**, 6-20. doi:10.1016/0378-5955(92)90164-I

Cai, T., Jen, H. I., Kang, H., Klisch, T. J., Zoghbi, H. Y. and Groves, A. K. (2015). Characterization of the transcriptome of nascent hair cells and identification of direct targets of the Atoh1 transcription factor. *J. Neurosci.* **35**, 5870-5883. doi:10.1523/JNEUROSCI.5083-14.2015

Camp, J. G., Badsha, F., Florio, M., Kanton, S., Gerber, T., Wilsch-Brauninger, M., Lewitus, E., Sykes, A., Hevers, W., Lancaster, M. et al. (2015). Human cerebral organoids recapitulate gene expression programs of fetal neocortex development. *Proc. Natl. Acad. Sci. USA* **112**, 15672-15677. doi:10.1073/pnas.1520760112

Chen, W., Cacciabue-Rivolta, D. I., Moore, H. D. and Rivolta, M. N. (2007). The human fetal cochlea can be a source for auditory progenitors/stem cells isolation. *Hear. Res.* **233**, 23-29. doi:10.1016/j.heares.2007.06.006

Costa, A., Sanchez-Guardado, L., Juniat, S., Gale, J. E., Daudet, N. and Henrique, D. (2015). Generation of sensory hair cells by genetic programming with a combination of transcription factors. *Development* **142**, 1948-1959. doi:10.1242/dev.119149

Cowan, C. S., Renner, M., De Gennaro, M., Gross-Scherf, B., Goldblum, D., Hou, Y., Munz, M., Rodrigues, T. M., Krol, J., Szikra, T. et al. (2020). Cell types of the human retina and its organoids at single-cell resolution. *Cell* **182**, 1623-1640.e34. doi:10.1016/j.cell.2020.08.013

De Bakker, B. S., De Jong, K. H., Hagoort, J., De Bree, K., Besselink, C. T., De Kanter, F. E., Veldhuis, T., Bais, B., Schildmeijer, R., Ruijter, J. M. et al.

(2016). An interactive three-dimensional digital atlas and quantitative database of human development. *Science* **354**, aag0053. doi:10.1126/science.aag0053

Denisenko, E., Guo, B. B., Jones, M., Hou, R., De Kock, L., Lassmann, T., Poppe, D., Clement, O., Simmons, R. K., Lister, R. et al. (2020). Systematic assessment of tissue dissociation and storage biases in single-cell and single-nucleus RNA-seq workflows. *Genome Biol.* **21**, 130. doi:10.1186/s13059-020-02048-6

Dincer, Z., Piao, J., Niu, L., Ganat, Y., Kriks, S., Zimmer, B., Shi, S. H., Tabar, V. and Studer, L. (2013). Specification of functional cranial placode derivatives from human pluripotent stem cells. *Cell Rep.* **5**, 1387-1402. doi:10.1016/j.celrep.2013.10.048

Durruthy-Durruthy, R., Gottlieb, A., Hartman, B. H., Waldhaus, J., Laske, R. D., Altman, R. and Heller, S. (2014). Reconstruction of the mouse otocyst and early neuroblast lineage at single-cell resolution. *Cell* **157**, 964-978. doi:10.1016/j.cell.2014.03.036

Ealy, M., Ellwanger, D. C., Kosaric, N., Stapper, A. P. and Heller, S. (2016). Single-cell analysis delineates a trajectory toward the human early otic lineage. *Proc. Natl. Acad. Sci. USA* **113**, 8508-8513. doi:10.1073/pnas.1605537113

Edgar, R., Domrachev, M. and Lash, A. E. (2002). Gene expression omnibus: NCBI gene expression and hybridization array data repository. *Nucleic Acids Res.* **30**, 207-210. doi:10.1093/nar/30.1.207

Elkon, R., Milon, B., Morrison, L., Shah, M., Vijayakumar, S., Racherla, M., Leitch, C. C., Silipino, L., Hadi, S., Weiss-Gayet, M. et al. (2015). RFX transcription factors are essential for hearing in mice. *Nat. Commun.* **6**, 8549. doi:10.1038/ncomms9549

Evsen, L., Sugahara, S., Uchikawa, M., Kondoh, H. and Wu, D. K. (2013). Progression of neurogenesis in the inner ear requires inhibition of Sox2 transcription by neurogenin1 and neurod1. *J. Neurosci.* **33**, 3879-3890. doi:10.1523/JNEUROSCI.4030-12.2013

Evtouchenko, L., Studer, L., Spenger, C., Dreher, E. and Seiler, R. W. (1996). A mathematical model for the estimation of human embryonic and fetal age. *Cell Transplant.* **5**, 453-464. doi:10.1177/096368979600500404

Germain, P., Lun, A., Macnair, W. and Robinson, M. (2021). Doublet identification in single-cell sequencing data using scDblFinder. *F1000Res.* **10**, 979. doi:10.12688/f1000research.73600.2

Goncalves, C. A., Larsen, M., Jung, S., Stratmann, J., Nakamura, A., Leuschner, M., Hersemann, L., Keshara, R., Perlman, S., Lundvall, L. et al. (2021). A 3D system to model human pancreas development and its reference single-cell transcriptome atlas identify signaling pathways required for progenitor expansion. *Nat. Commun.* **12**, 3144. doi:10.1038/s41467-021-23295-6

Groves, A. K. and Fekete, D. M. (2012). Shaping sound in space: the regulation of inner ear patterning. *Development* **139**, 245-257. doi:10.1242/dev.067074

Gu, R., Brown, R. M., 2nd, Hsu, C. W., Cai, T., Crowder, A. L., Piazza, V. G., Vadakkan, T. J., Dickinson, M. E. and Groves, A. K. (2016). Lineage tracing of Sox2-expressing progenitor cells in the mouse inner ear reveals a broad contribution to non-sensory tissues and insights into the origin of the organ of Corti. *Dev. Biol.* **414**, 72-84. doi:10.1016/j.ydbio.2016.03.027

Hang, J., Pan, W., Chang, A., Li, S., Li, C., Fu, M. and Tang, J. (2016). Synchronized progression of prestin expression and auditory brainstem response during postnatal development in rats. *Neural Plast.* **2016**, 4545826. doi:10.1155/2016/4545826

Haniffa, M., Taylor, D., Linnarsson, S., Aronow, B. J., Bader, G. D., Barker, R. A., Camara, P. G., Camp, J. G., Chedotal, A., Copp, A. et al. (2021). A roadmap for the human developmental cell atlas. *Nature* **597**, 196-205. doi:10.1038/s41586-021-03620-1

Hao, Y., Hao, S., Andersen-Nissen, E., Mauck, W. M., 3rd, Zheng, S., Butler, A., Lee, M. J., Wilk, A. J., Darby, C., Zager, M. et al. (2021). Integrated analysis of multimodal single-cell data. *Cell* **184**, 3573-3587.e29. doi:10.1016/j.cell.2021.04.048

Hartman, B. H., Durruthy-Durruthy, R., Laske, R. D., Losorelli, S. and Heller, S. (2015). Identification and characterization of mouse otic sensory lineage genes. *Front. Cell Neurosci.* **9**, 79. doi:10.3389/fncel.2015.00079

Hartman, B. H., Bscke, R., Ellwanger, D. C., Keymeulen, S., Scheibinger, M. and Heller, S. (2018). Fbxo2(VHC) mouse and embryonic stem cell reporter lines delineate in vitro-generated inner ear sensory epithelia cells and enable otic lineage selection and Cre-recombination. *Dev. Biol.* **443**, 64-77. doi:10.1016/j.ydbio.2018.08.013

Hatakeyama, M., Opitz, L., Russo, G., Qi, W., Schlapbach, R. and Rehrauer, H. (2016). SUSHI - an exquisite recipe for fully documented, reproducible and reusable NGS data analysis. *BMC Bioinformatics* **17**, 228. doi:10.1186/s12859-016-1104-8

Hidalgo-Sanchez, M., Alvarado-Mallart, R. and Alvarez, I. S. (2000). Pax2, Otx2, Gbx2 and Fgf8 expression in early otic vesicle development. *Mech. Dev.* **95**, 225-229. doi:10.1016/S0925-4773(00)00332-4

Johnson Chacko, L., Sergi, C., Eberharter, T., Dudas, J., Rask-Andersen, H., Hoermann, R., Fritsch, H., Fischer, N., Glueckert, R. and Schrott-Fischer, A. (2020). Early appearance of key transcription factors influence the spatiotemporal development of the human inner ear. *Cell Tissue Res.* **379**, 459-471. doi:10.1007/s00441-019-03115-6

Kaiser, M., Wojahn, I., Rudat, C., Ludtke, T. H., Christoffels, V. M., Moon, A., Kispert, A. and Trowe, M. O. (2021). Regulation of otocyst patterning by Tbx2 and Tbx3 is required for inner ear morphogenesis in the mouse. *Development* **148**, dev195651. doi:10.1242/dev.195651

Kiernan, A. E., Pelling, A. L., Leung, K. K., Tang, A. S., Bell, D. M., Tease, C., Lovell-Badge, R., Steel, K. P. and Cheah, K. S. (2005). Sox2 is required for sensory organ development in the mammalian inner ear. *Nature* **434**, 1031-1035. doi:10.1038/nature03487

Koehler, K. R., Mikosz, A. M., Molosh, A. I., Patel, D. and Hashino, E. (2013). Generation of inner ear sensory epithelia from pluripotent stem cells in 3D culture. *Nature* **500**, 217-221. doi:10.1038/nature12298

Koehler, K. R., Nie, J., Longworth-Mills, E., Liu, X. P., Lee, J., Holt, J. R. and Hashino, E. (2017). Generation of inner ear organoids containing functional hair cells from human pluripotent stem cells. *Nat. Biotechnol.* **35**, 583-589. doi:10.1038/nbt.3840

Kolla, L., Kelly, M. C., Mann, Z. F., Anaya-Rocha, A., Ellis, K., Lemons, A., Palermo, A. T., So, K. S., Mays, J. C., Orvis, J. et al. (2020). Characterization of the development of the mouse cochlear epithelium at the single cell level. *Nat. Commun.* **11**, 2389. doi:10.1038/s41467-020-16113-y

Lancaster, M. A., Renner, M., Martin, C. A., Wenzel, D., Bicknell, L. S., Hurles, M. E., Homfray, T., Penninger, J. M., Jackson, A. P. and Knoblich, J. A. (2013). Cerebral organoids model human brain development and microcephaly. *Nature* **501**, 373-379. doi:10.1038/nature12517

Lavigne-Rebillard, M. and Pujol, R. (1986). Development of the auditory hair cell surface in human fetuses. A scanning electron microscopy study. *Anat. Embryol.* **174**, 369-377. doi:10.1007/BF00698787

Lavigne-Rebillard, M. and Pujol, R. (1987). Surface aspects of the developing human organ of Corti. *Acta Otolaryngol. Suppl.* **436**, 43-50. doi:10.3109/00016488709124975

Lavigne-Rebillard, M. and Pujol, R. (1988). Hair cell innervation in the fetal human cochlea. *Acta Otolaryngol.* **105**, 398-402. doi:10.3109/00016488809119492

Leger, S. and Brand, M. (2002). Fgf8 and Fgf3 are required for zebrafish ear placode induction, maintenance and inner ear patterning. *Mech. Dev.* **119**, 91-108. doi:10.1016/S0925-4773(02)00343-X

Li, Y., Liu, H., Giffen, K. P., Chen, L., Beisel, K. W. and He, D. Z. Z. (2018). Transcriptomes of cochlear inner and outer hair cells from adult mice. *Sci. Data* **5**, 180199. doi:10.1038/sdata.2018.199

Litsiou, A., Hanson, S. and Streit, A. (2005). A balance of FGF, BMP and WNT signalling positions the future placode territory in the head. *Development* **132**, 4051-4062. doi:10.1242/dev.01964

Locher, H., Frijns, J. H., Van Iperen, L., De Groot, J. C., Huisman, M. A. and Chuva De Sousa Lopes, S. M. (2013). Neurosensory development and cell fate determination in the human cochlea. *Neural Dev.* **8**, 20. doi:10.1186/1749-8104-8-20

Locher, H., De Groot, J. C., Van Iperen, L., Huisman, M. A., Frijns, J. H. and Chuva De Sousa Lopes, S. M. (2014). Distribution and development of peripheral glial cells in the human fetal cochlea. *Plos One* **9**, e88066. doi:10.1371/journal.pone.0088066

Locher, H., De Groot, J. C., Van Iperen, L., Huisman, M. A., Frijns, J. H. and Chuva De Sousa Lopes, S. M. (2015). Development of the stria vascularis and potassium regulation in the human fetal cochlea: insights into hereditary sensorineural hearing loss. *Dev. Neurobiol.* **75**, 1219-1240. doi:10.1002/dneu.22279

Luo, X. J., Deng, M., Xie, X., Huang, L., Wang, H., Jiang, L., Liang, G., Hu, F., Tieu, R., Chen, R. et al. (2013). GATA3 controls the specification of prosensory domain and neuronal survival in the mouse cochlea. *Hum. Mol. Genet.* **22**, 3609-3623. doi:10.1093/hmg/ddt212

Maroon, H., Walshe, J., Mahmood, R., Kiefer, P., Dickson, C. and Mason, I. (2002). Fgf3 and Fgf8 are required together for formation of the otic placode and vesicle. *Development* **129**, 2099-2108. doi:10.1242/dev.129.9.2099

Martik, M. L. and Bronner, M. E. (2021). Riding the crest to get a head: neural crest evolution in vertebrates. *Nat. Rev. Neurosci.* **22**, 616-626. doi:10.1038/s41583-021-00503-2

Martin, K. and Groves, A. K. (2006). Competence of cranial ectoderm to respond to Fgf signaling suggests a two-step model of otic placode induction. *Development* **133**, 877-887. doi:10.1242/dev.02267

Mccarthy, D. J., Campbell, K. R., Lun, A. T. L. and Willis, Q. F. (2017). Scater: pre-processing, quality control, normalisation and visualisation of single-cell RNA-seq data in R. *Bioinformatics* **33**, 1179-1186. doi:10.1093/bioinformatics/btw777

Mendez-Maldonado, K., Vega-Lopez, G. A., Aybar, M. J. and Velasco, I. (2020). Neurogenesis from neural crest cells: molecular mechanisms in the formation of cranial nerves and Ganglia. *Front. Cell Dev. Biol.* **8**, 635. doi:10.3389/fcell.2020.00635

Menendez, L., Trecek, T., Gopalakrishnan, S., Tao, L., Markowitz, A. L., Yu, H. V., Wang, X., Llamas, J., Huang, C., Lee, J. et al. (2020). Generation of inner ear hair cells by direct lineage conversion of primary somatic cells. *eLife* **9**, e55249. doi:10.7554/eLife.55249

Moore, S. T., Nakamura, T., Nie, J., Solivais, A. J., Aristizábal-Ramírez, I., Ueda, Y., Mayakannan, M., Reddy, V. S., Romano, D. R., Perrin, B. J. et al. (2022). Generating high-fidelity cochlear organoids from human pluripotent stem cells. *Cell Stem Cell* **30**, 950-961. doi:10.1016/j.stem.2023.06.006

Munnamalai, V. and Fekete, D. M. (2017). Building the human inner ear in an organoid. *Nat. Biotechnol.* **35**, 518-520. doi:10.1038/nbt.3899
Nie, J. and Hashino, E. (2020). Generation of inner ear organoids from human pluripotent stem cells. *Methods Cell Biol.* **159**, 303-321. doi:10.1016/bs.mcb.2020.02.006
Nie, J., Ueda, Y., Solivais, A. J. and Hashino, E. (2022). CHD7 regulates otic lineage specification and hair cell differentiation in human inner ear organoids. *Nat. Commun.* **13**, 7053. doi:10.1038/s41467-022-34759-8
Nist-Lund, C., Kim, J. and Koehler, K. R. (2022). Advancements in inner ear development, regeneration, and repair through otic organoids. *Curr. Opin. Genet. Dev.* **76**, 101954. doi:10.1016/j.gde.2022.101954
Noda, T., Meas, S. J., Nogami, J., Amemiya, Y., Uchi, R., Ohkawa, Y., Nishimura, K. and Dabdoub, A. (2018). Direct reprogramming of spiral ganglion non-neuronal cells into neurons: toward ameliorating sensorineural hearing loss by gene therapy. *Front. Cell Dev. Biol.* **6**, 16. doi:10.3389/fcell.2018.00016
O'Rahilly, R. (1963). The early development of the otic vesiclein staged human embryos. *J. Embryol. Exp. Morphol.* **11**, 741-755.
Pechriggl, E. J., Bitsche, M., Glueckert, R., Rask-Andersen, H., Blumer, M. J., Schrott-Fischer, A. and Fritsch, H. (2015). Development of the innervation of the human inner ear. *Dev. Neurobiol.* **75**, 683-702. doi:10.1002/dneu.22242
Petitpre, C., Faure, L., Uhl, P., Fontanet, P., Filova, I., Pavlinkova, G., Adameyko, I., Hadjab, S. and Lallemend, F. (2022). Single-cell RNA-sequencing analysis of the developing mouse inner ear identifies molecular logic of auditory neuron diversification. *Nat. Commun.* **13**, 3878. doi:10.1038/s41467-022-31580-1
Pollen, A. A., Bhaduri, A., Andrews, M. G., Nowakowski, T. J., Meyerson, O. S., Mostajo-Radji, M. A., Di Lullo, E., Alvarado, B., Bedolli, M., Dougherty, M. L. et al. (2019). Establishing cerebral organoids as models of human-specific brain evolution. *Cell* **176**, 743-756.e17. doi:10.1016/j.cell.2019.01.017
Pujol, R. and Lavigne-Rebillard, M. (1985). Early stages of innervation and sensory cell differentiation in the human fetal organ of Corti. *Acta Otolaryngol. Suppl.* **423**, 43-50. doi:10.3109/00016488509122911
Puligilla, C., Dabdoub, A., Brenowitz, S. D. and Kelley, M. W. (2010). Sox2 induces neuronal formation in the developing mammalian cochlea. *J. Neurosci.* **30**, 714-722. doi:10.1523/JNEUROSCI.3852-09.2010
Qi, Y., Zhang, X. J., Renier, N., Wu, Z., Atkin, T., Sun, Z., Ozair, M. Z., Tchieu, J., Zimmer, B., Fattahi, F. et al. (2017). Combined small-molecule inhibition accelerates the derivation of functional cortical neurons from human pluripotent stem cells. *Nat. Biotechnol.* **35**, 154-163. doi:10.1038/nbt.3777
Radde-Gallwitz, K., Pan, L., Gan, L., Lin, X., Segil, N. and Chen, P. (2004). Expression of Islet1 marks the sensory and neuronal lineages in the mammalian inner ear. *J. Comp. Neurol.* **477**, 412-421. doi:10.1002/cne.20257
Ranum, P. T., Goodwin, A. T., Yoshimura, H., Kolbe, D. L., Walls, W. D., Koh, J. Y., He, D. Z. Z. and Smith, R. J. H. (2019). Insights into the biology of hearing and deafness revealed by single-cell RNA sequencing. *Cell Rep.* **26**, 3160-3171.e3. doi:10.1016/j.celrep.2019.02.053
Renauld, J. M., Khan, V. and Basch, M. L. (2022). Intermediate cells of dual embryonic origin follow a basal to apical gradient of ingression into the lateral wall of the Cochlea. *Front. Cell Dev. Biol.* **10**, 867153. doi:10.3389/fcell.2022.867153
Riccomagno, M. M., Takada, S. and Epstein, D. J. (2005). Wnt-dependent regulation of inner ear morphogenesis is balanced by the opposing and supporting roles of Shh. *Genes Dev.* **19**, 1612-1623. doi:10.1101/gad.1303905
Roccio, M. (2021). Directed differentiation and direct reprogramming: applying stem cell technologies to hearing research. *Stem Cells* **39**, 375-388. doi:10.1002/stem.3315
Roccio, M. and Edge, A. S. B. (2019). Inner ear organoids: new tools to understand neurosensory cell development, degeneration and regeneration. *Development* **146**, dev177188. doi:10.1242/dev.177188
Roccio, M., Perny, M., Ealy, M., Widmer, H. R., Heller, S. and Senn, P. (2018). Molecular characterization and prospective isolation of human fetal cochlear hair cell progenitors. *Nat. Commun.* **9**, 4027. doi:10.1038/s41467-018-06334-7
Saint-Jeannet, J. P. and Moody, S. A. (2014). Establishing the pre-placodal region and breaking it into placodes with distinct identities. *Dev. Biol.* **389**, 13-27. doi:10.1016/j.ydbio.2014.02.011
Sans, A. and Dechesne, C. (1985). Early development of vestibular receptors in human embryos. An electron microscopic study. *Acta Otolaryngol. Suppl.* **423**, 51-58. doi:10.3109/00016488509122912
Scheffer, D. I., Shen, J., Corey, D. P. and Chen, Z. Y. (2015). Gene expression by mouse inner ear hair cells during development. *J. Neurosci.* **35**, 6366-6380. doi:10.1523/JNEUROSCI.5126-14.2015
Schindelin, J., Arganda-Carreras, I., Frise, E., Kaynig, V., Longair, M., Pietzsch, T., Preibisch, S., Rueden, C., Saalfeld, S., Schmid, B. et al. (2012). Fiji: an open-source platform for biological-image analysis. *Nat. Methods* **9**, 676-682. doi:10.1038/nmeth.2019
Senn, P., Mina, A., Volkenstein, S., Kranebitter, V., Oshima, K. and Heller, S. (2019). Progenitor cells from the adult human inner ear. *Anat. Rec.* **303**, 461-470. doi:10.1002/ar.24228
Shengyang Yu, K., Frumm, S. M., Park, J. S., Lee, K., Wong, D. M., Byrnes, L., Knox, S. M., Sneddon, J. B. and Tward, A. D. (2019). Development of the mouse and human cochlea at single cell resolution. *bioRxiv*. https://www.biorxiv.org/content/10.1101/739680v2.
Soldatov, R., Kaucka, M., Kastriti, M. E., Petersen, J., Chontorotzea, T., Englmaier, L., Akkuratova, N., Yang, Y., Haring, M., Dyachuk, V. et al. (2019). Spatiotemporal structure of cell fate decisions in murine neural crest. *Science* **364**, eaas9536. doi:10.1126/science.aas9536
Steel, K. P. and Barkway, C. (1989). Another role for melanocytes: their importance for normal stria vascularis development in the mammalian inner ear. *Development* **107**, 453-463. doi:10.1242/dev.107.3.453
Steevens, A. R., Sookiasian, D. L., Glatzer, J. C. and Kiernan, A. E. (2017). SOX2 is required for inner ear neurogenesis. *Sci. Rep.* **7**, 4086. doi:10.1038/s41598-017-04315-2
Steinhart, M. R., van der Valk, W. H., Osorio, D., Serdy, S. A., Zhang, J., Nist-Lund, C., Kim, J., Moncada-Reid, C., Sun, L., Lee, J. and Koehler, K. R. (2023). Mapping oto-pharyngeal development in a human inner ear organoid model. *Development* **150**, dev201871. doi:10.1242/dev.201871
Steventon, B., Mayor, R. and Streit, A. (2012). Mutual repression between Gbx2 and Otx2 in sensory placodes reveals a general mechanism for ectodermal patterning. *Dev. Biol.* **367**, 55-65. doi:10.1016/j.ydbio.2012.04.025
Steventon, B., Mayor, R. and Streit, A. (2014). Neural crest and placode interaction during the development of the cranial sensory system. *Dev. Biol.* **389**, 28-38. doi:10.1016/j.ydbio.2014.01.021
Stuart, T., Butler, A., Hoffman, P., Hafemeister, C., Papalexi, E., Mauck, W. M., 3rd, Hao, Y., Stoeckius, M., Smibert, P. and Satija, R. (2019). Comprehensive integration of single-cell data. *Cell* **177**, 1888-1902.e1821. doi:10.1016/j.cell.2019.05.031
Sun, Y., Wang, L., Zhu, T., Wu, B., Wang, G., Luo, Z., Li, C., Wei, W. and Liu, Z. (2022). Single-cell transcriptomic landscapes of the otic neuronal lineage at multiple early embryonic ages. *Cell Rep.* **38**, 110542. doi:10.1016/j.celrep.2022.110542
Taylor, R. R., Jagger, D. J., Saeed, S. R., Axon, P., Donnelly, N., Tysome, J., Moffatt, D., Irving, R., Monksfield, P., Coulson, C. et al. (2015). Characterizing human vestibular sensory epithelia for experimental studies: new hair bundles on old tissue and implications for therapeutic interventions in ageing. *Neurobiol. Aging* **36**, 2068-2084. doi:10.1016/j.neurobiolaging.2015.02.013
Uniken Venema, W. T. C., Ramirez-Sanchez, A. D., Bigaeva, E., Withoff, S., Jonkers, I., Mcintyre, R. E., Ghouraba, M., Raine, T., Weersma, R. K., Franke, L. et al. (2022). Gut mucosa dissociation protocols influence cell type proportions and single-cell gene expression levels. *Sci. Rep.* **12**, 9897. doi:10.1038/s41598-022-13812-y
Van Der Valk, W. H., Steinhart, M. R., Zhang, J. and Koehler, K. R. (2021). Building inner ears: recent advances and future challenges for in vitro organoid systems. *Cell Death Differ.* **28**, 24-34. doi:10.1038/s41418-020-00678-8
Van Der Valk, W. H., Van Beelen, E. S. A., Steinhart, M. R., Nist-Lund, C., Osorio, D., De Groot, J., Sun, L., Van Benthem, P. P. G., Koehler, K. R. and Locher, H. (2023). A single-cell level comparison of human inner ear organoids with the human cochlea and vestibular organs. *Cell Rep.* **42**, 112623. doi:10.1016/j.celrep.2023.112623
Wahle, P., Brancati, G., Harmel, C., He, Z., Gut, G., Del Castillo, J. S., Xavier Da Silveira Dos Santos, A., Yu, Q., Noser, P., Fleck, J. S. et al. (2023). Multimodal spatiotemporal phenotyping of human retinal organoid development. *Nat. Biotechnol.* doi:10.1038/s41587-023-01747-2
Waldhaus, J., Durruthy-Durruthy, R. and Heller, S. (2015). Quantitative high-resolution cellular map of the organ of Corti. *Cell Rep.* **11**, 1385-1399. doi:10.1016/j.celrep.2015.04.062
Wang, T., Ling, A. H., Billings, S. E., Hosseini, D. K., Vaisbuch, Y., Kim, G. S., Atkinson, P. J., Sayyid, Z. N., Aaron, K. A., Wagh, D. et al. (2022). Single-cell transcriptomic atlas reveals increased regeneration in diseased human inner ears. *bioRxiv*. doi:10.1101/2022.10.29.514378
Wilkerson, B. A., Zebroski, H. L., Finkbeiner, C. R., Chitsazan, A. D., Beach, K. E., Sen, N., Zhang, R. C. and Bermingham-Mcdonogh, O. (2021). Novel cell types and developmental lineages revealed by single-cell RNA-seq analysis of the mouse crista ampullaris. *eLife* **10**, e60108. doi:10.7554/eLife.60108
Wilson, P. A. and Hemmati-Brivanlou, A. (1995). Induction of epidermis and inhibition of neural fate by Bmp-4. *Nature* **376**, 331-333. doi:10.1038/376331a0
Wiwatpanit, T., Lorenzen, S. M., Cantu, J. A., Foo, C. Z., Hogan, A. K., Marquez, F., Clancy, J. C., Schipma, M. J., Cheatham, M. A., Duggan, A. et al. (2018). Trans-differentiation of outer hair cells into inner hair cells in the absence of INSM1. *Nature* **563**, 691-695. doi:10.1038/s41586-018-0570-8
Wu, D. K. and Kelley, M. W. (2012). Molecular mechanisms of inner ear development. *Cold Spring Harb. Perspect. Biol.* **4**, a008409. doi:10.1101/cshperspect.a008409
Xu, Y., Zhang, T., Zhou, Q., Hu, M., Qi, Y., Xue, Y., Nie, Y., Wang, L., Bao, Z. and Shi, W. (2023). A single-cell transcriptome atlas profiles early organogenesis in human embryos. *Nat. Cell Biol.* **25**, 604-615. doi:10.1038/s41556-023-01108-w
Yasuda, M., Yamada, S., Uwabe, C., Shiota, K. and Yasuda, Y. (2007). Three-dimensional analysis of inner ear development in human embryos. *Anat. Sci. Int.* **82**, 156-163. doi:10.1111/j.1447-073X.2007.00176.x
Zelarayan, L. C., Vendrell, V., Alvarez, Y., Dominguez-Frutos, E., Theil, T., Alonso, M. T., Maconochie, M. and Schimmang, T. (2007). Differential requirements for FGF3, FGF8 and FGF10 during inner ear development. *Dev. Biol.* **308**, 379-391. doi:10.1016/j.ydbio.2007.05.033